Precambrian Research 360 (2021) 106243

Contents lists available at ScienceDirect

Precambrian Research

journal homepage: www.elsevier.com/locate/precamres

New high-quality paleomagnetic data from the Borborema Province (NE Brazil): Refinement of the APW path of Gondwana in the Early Cambrian

Paul Yves Jean Antonio *, Ricardo Ivan Ferreira Trindade, Bruno Giacomini, Daniele Brandt, Eric Tohver

Instituto de Astronomia, Geofísica e Ciências Atmosféricas (IAG), Universidade de São Paulo (USP), Rua do Matão, 1226, 05508-090 São Paulo, SP, Brazil

ARTICLE INFO

Keywords:
Neoproterozoic
West Gondwana
Cambrian
True polar wander

ABSTRACT

The Neoproterozoic-Paleozoic transition (~541 Ma) was a turning point in Earth's history resulting in great biological changes between the microbial Precambrian life and the Ediacaran biotic revolution with the occupation of the sedimentary substrate, the dawn of biomineralization and the appearance of the earliest multicellular organisms. In parallel, this period is marked by a large plate reorganization leading to the assembly of Gondwana and by major climatic changes (extreme glacial events). Due in part to a poor paleomagnetic database for the different cratons in the Ediacarian-Cambrian times, the global paleogeography at that time remains controversial. In this study we present a new high-quality paleomagnetic pole (R = 7) for the Monteiro dyke swarm in the Borborema Province (NE Brazil) located at 18.2°S and 344.9°E (A95 = 11.7° K = 9.3). They are fine-grained hornblende dolerite dated by U-Pb on zircon at ~538 Ma. Rock magnetic data indicate that magnetite and pyrrhotite are the main remanence carriers. Positive baked-contact tests support the primary remanence obtained for these dykes (19 sites). A positive reversal test (classified C) was also obtained from the 14 sites with negative inclination and the 5 sites with positive inclination, indicating that the paleosecular variation was eliminated. Our new key pole is not consistent with the classical apparent polar wander path of the Gondwana which consists of a long track from a southern polar position at ~590 Ma to an equatorial position at ~520 Ma, and suggests instead rapid and small oscillations of the APW, after the end of the large IITPW at *ca.* 560 Ma. These TPWs are supposedly caused by changes in the inertia tensor of the Earth due to internal mass redistribution, related to rapid changes in subduction velocity. Links of these rapid oscillations and the timing of the Cambrian radiation could be crucial to understand the early history of animal life

1. Introduction

The Neoproterozoic Era is marked by the first complex animals, extreme ice ages (Snowball Earth events) and the rise of oxygen in the atmosphere (Hoffman and Schrag, 2002; Kirschvink, 1992; Kirschvink et al., 1997; Knoll, 1992). Major changes in Earth's geodynamics appear with emergence of modern-style plate tectonics marked by the appearance of common ophiolites, blueschists and ultra-high-pressure metamorphic conditions (Stern, 2005). These major changes occurred between the breakup of the Rodinia supercontinent (~850 Ma) and the final assembly of the Gondwana landmass at ~520 Ma (Cawood and Pisarevsky, 2017; Dalziel, 1997; Hoffman, 1991; Pisarevsky et al., 2008; Stern, 2008). The assembly of West Gondwana is related to the development of the Iapetus Ocean and the closure of Goias-Pharusian and Clymene oceans but the paleogeography at the Ediacaran-Cambrian transition is poorly known with few well-determined paleomagnetic constraints (Buchan et al., 2001; Meert and Powell, 2001; Tohver et al., 2006).

The paleomagnetic data necessary to resolve the paleogeography of the Ediacaran-Cambrian transition is also of interest to understand the unusual Ediacaran geomagnetic field behavior (Bazhenov et al., 2016; Gallet and Pavlov, 2016; Bono et al., 2019). Indeed, the interval ~600–500 Ma shows a paleomagnetic scattering pattern with many discordant poles for different continents, such as Laurentia, Baltica, Australia and West Africa. To reconciliate these discordant paleomagnetic data, the occurrence of rapid true polar wander (TPW) or inertial interchange true polar wander (IITPW, or Type II-TPW according to Raub et al. (2007)) episodes weres invoked. An IITPW event describes the ~90° motion in amplitude of the entire solid earth (mantle and crust) in respect to the spin axis of the Earth (Goldreich and Toomre,

* Corresponding author.
E-mail address: paulantonio0931@gmail.com (P.Y.J. Antonio).

https://doi.org/10.1016/j.precamres.2021.106243
Received 23 October 2020; Received in revised form 15 April 2021; Accepted 19 April 2021
Available online 10 May 2021

1969; Kirschvink et al., 1997; Rose and Buffett, 2017). These movements of the Earth's rotation pole (TPW) are the consequences of the internal redistribution of mass changing the moment of inertia of the planet (Raub et al., 2007). During the Ediacarian-Cambrian transition such events were described with: (1) two inertial interchange TPW (IITPW) between 615 and 571 Ma and between 571 and 565 Ma (Robert et al., 2017), and (2) a TPW in the Lower Cambrian between 550 and 505 Ma (Kirschvink et al., 1997; Meert, 1999; Mitchell et al., 2010). More recently, this late Cambrian TPW (~505–495 Ma) was also invoked when analyzing paleomagnetic poles from South China (Jiao et al., 2018). TPW oscillations between 615 and 530 Ma were related to the circum-Sutton plume activity located at the north-eastern border of the Laurentia (Mitchell et al., 2011). In order to test the presence of these TPW events, Torsvik et al. (1998) highlighted the importance of having high-quality reference poles. Another point of view is explaining such uncommon paleomagnetic results with a geomagnetic field incompatible to the geocentric axial dipole model. The shifting between shallow and steep paleomagnetic directions found for Ediacaran rocks of similar ages from Baltica could be also explained by an alternation between a co-axial and equatorial alignment the geomagnetic dipole (Abrajevitch and Van der Voo, 2010). Magnetostratigraphic data reveal extreme reversals frequency (>20 R/Ma) during the Lower Cambrian (~550–500 Ma) for Baltica, China, and the Siberia (Bazhenov et al., 2016; Duan et al., 2018; Gallet et al., 2003, 2019; Gallet and Pavlov, 2016). In addition, high-quality paleointensity data indicate a time-averaged dipole moment as low as ~0.7 × 10^{22} A.m^2 for the ~565 Ma Sept-îles intrusive (Bono et al., 2019) and confirms previous results for the same unit (Bono and Tarduno, 2015). High-reversal frequency and ultra-low intensity of the geomagnetic field can be associated with the late Neoproterozoic inner-core nucleation hypothesis (Bono et al., 2019; Driscoll and Evans, 2016; Landeau et al., 2017; Lhuillier et al., 2019). A weak magnetosphere during the Ediacaran could also enhance the planet's exposure to solar radiation and a possible link with the late Ediacaran to Cambrian metazoan diversification (Meert et al., 2016).

In this work, we provide new paleomagnetic results for the Ediacaran-Cambrian Monteiro dyke swarm of the Borborema Province (NE Brazil) in South America. Our investigation was motivated to obtain a first paleomagnetic pole that passes a positive baked contact to characterize the Ediacaran-Cambrian transition (~542 Ma) for South America. Combined with the ~520 Ma Itabaiana key pole (Trindade et al., 2006) of the same tectonic province, our new result will help to refine the Apparent Polar Wander Path of Gondwana and testing the possibility of TPW oscillations during the Early-Mid-Cambrian.

2. Geological setting

The Borborema Province (BP) is a complex orogenic system comprised between the São Francisco craton in south and the Parnaiba basin to the northwest (Almeida et al., 1981; Neves et al., 2000; Santos et al., 2018). It represents an area of ~450,000 km^2 formed of discontinuous remnants of Archean and Paleoproterozoic migmatitic gneiss complexes, and Neoproterozoic supracrustal rocks (Neves et al., 2000; Van Schmus et al., 2008, 2011). The main structural feature of the BP is a network of strike-slip shear zones that rework a flat-lying gneissic foliation (Vauchez et al., 1995). In the paleogeographical frame, the Borborema Province represents the continuation in South-America of the Pan-African mobile belts of Western Africa that sealed the northern part of Gondwana during the Neoproterozoic Brasiliano/Pan-African orogeny (Arthaud et al., 2008; Neves et al., 2000; Caby et al., 1990; Cordani et al., 2013a; Davison and Dos Santos, 1989; Ganade et al., 2016; Ganade de Araujo et al., 2014a, 2014b; Van Schmus et al., 2008).

The Borborema Province can be divided into three major domains separated by continental-scale transcurrent shear zones (Fig. 1). The Patos shear zone marks the separation between the Northern subprovince and the Central subprovince, also called the Transversal domain (Van Schmus et al., 2011). A main characteristic of the Central domain is the recognition of the ~1000–920 Ma Cariris Velhos event (Dantas et al., 2019; dos Santos et al., 2010). The Southern subprovince is comprised between the Pernamabuco shear zone and the São Francisco craton and is composed of various blocks or domains ranging in age from Archean to Neoproterozoic. The study area is located in the Central domain near to Monteiro city (Paraíba State, Figs. 1 and 2-A). The basement is made up of Paleoproterozoic metamorphic units (~2200–2000 Ma) which were reworked during the Cariris Velhos event (Fig. 2-A). The basement of the Central domain was deformed during the Pan-African/Brasiliano orogeny with the reactivation of shear zones associated to a voluminous granitic plutonism with ages ranging between 600 and 520 Ma, the Neoproterozoic Cariri magmatic complex (Hollanda et al., 2010b). The mean deformation in the Monteiro area is related with the activity of the dextral Coxixola shear zone which flanked the northern limit of the Sumé syenogranite (Santos and Santos, 2019). This shear zone continues in the Cameroon Shield in Africa and represents an important structural element of correlation across the Atlantic Ocean (de Wit et al., 2008). Timing of metamorphic cooling

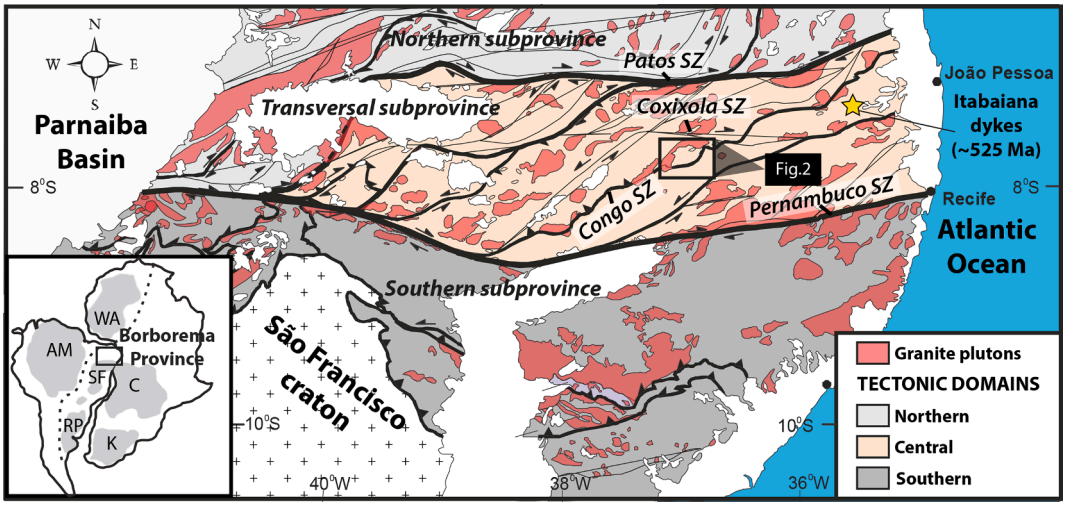

Fig. 1. Inset: Localization of the Borborema Province before the separation with West Africa. Tectonic framework of the Borborema Province with indication of main shear zones (Patos S.Z., Coxixola S.Z., Congo S.Z. and Pernambuco S.Z.), modified from Archanjo et al. (2008). Location of the two mafic dyke swarm where a key paleomagnetic pole was calculated for the Borborema Province: the ~538 Ma Monteiro dykes (Fig. 2, this study) and the ~525 Ma Itabaiana dykes (star) (Trindade et al., 2006).

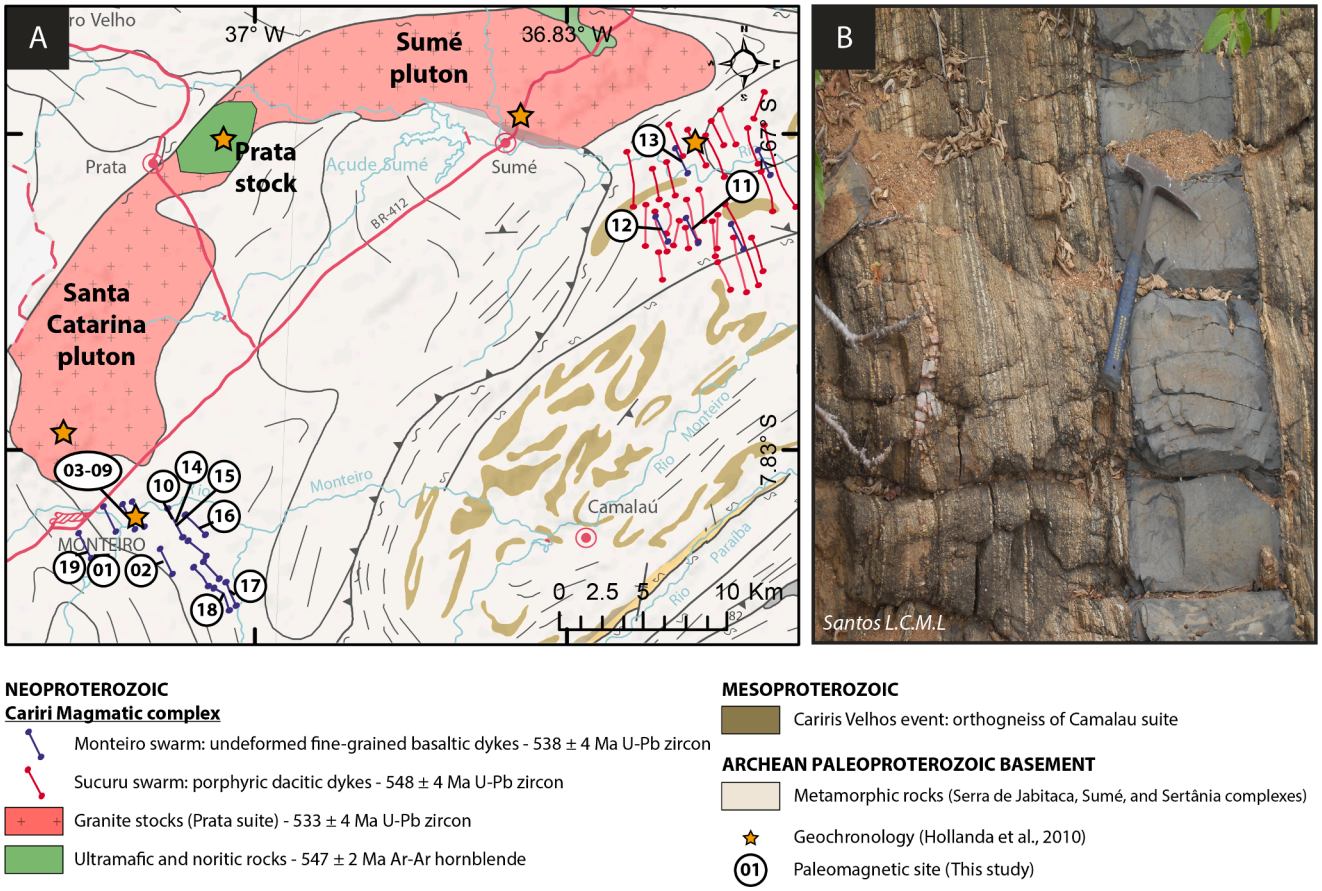

Fig. 2. **A:** Geological map showing the location of the Monteiro (this study) and Sucuru dyke swarms, and geochronological sites (Hollanda et al., 2010a). The Cariri Magmatic Complex is represented by the Santa Catarina, the Sumé plutons and the associated dykes. **B:** Field aspect for one undeformed fine-grained basaltic andesite dyke (KL11) within the area of Sucuru, and therefore considered as coeval with the Monteiro dyke swarm. Courtesy of Santos L.C.M.L for sharing the photography.

following the deformation along the Coxixola shear zone is provided by the $^{40}Ar/^{39}Ar$ ages for muscovite single crystals of mylonitic rocks of upper greenschist to lower amphibolite facies. In this area, muscovite ages of mylonites show two plateau-age at ~546 and 510 Ma (Hollanda et al., 2010b) which constrain the tectonic exhumation.

In the Monteiro area, the Cariri Magmatic event includes the Prata gabbro-norite stock (547 ± 2 Ma Ar-Ar hornblende) coeval with the NW-trending Sucuru dyke swarm, well-dated at 548 ± 4 Ma by U-Pb SHRIMP (Hollanda et al., 2010b). This ~550 Ma magmatic pulse was followed by the emplacement of the Sumé and Santa Catarina syenogranites at 534 ± 3 Ma and 533 ± 5 (U-Pb SHRIMP ages), respectively (Hollanda et al., 2010b). The NW- trending Monteiro dykes yielded one age of 538 ± 4 Ma by U-Pb SHRIMP and were considered coeval with the syenogranitic stocks (Hollanda et al., 2010b). The Ar-Ar age on biotite of 530 ± 2 Ma for the Prata mafic stock can indicate a slow cooling, or a possible re-heating at ~530 Ma (Hollanda et al., 2010b). Thus, in this area the thermal influence of the Cariri Magmatic event spanned at least 20 Ma.

The NW- trending Sucuru (548 ± 4 Ma) and Monteiro (538 ± 4 Ma) dyke swarms are intrusive into the Archean-Paleoproterozoic gneissic basement near to the terminations of the Sumé and Santa Catarina plutons (533 ± 4 Ma), respectively (Fig. 2-A). They are vertical dykes, ~0.10 m to 20 m in width and typically between 100 and 500 m in length (Fig. 2-B). These dykes are basaltic andesite (or dolerite), dacite, or andesitic rocks. Fine-grained doleritic dykes are composed of Ca-plagioclase, pyroxene, hornblende, rare olivine and Fe-Ti oxides. Porphyric andesitic dykes are composed of large plagioclase, augite, hornblende, rare quartz and Fe-Ti oxides. Deformation is a common feature in the Sucuru dykes, in opposition to the Monteiro dykes sampled for this paleomagnetic study.

3. Sampling and laboratory procedures

For this paleomagnetic study we collected samples on 19 sites of the Monteiro dyke swarm, comprising 16 sites near Monteiro city and 3 undeformed dykes located within the Sucuru area (KL11, KL12 and KL13) (Table 1; Fig. 2). Thickness of the NW- trending dykes vary between 0.15 m (KL07) and 8 m (KL09). In addition, for 4 sites of Monteiro dykes, we also sampled the host basement rocks for baked contact tests (KL03, KL04, KL05, KL06). Paleomagnetic samples were collected using a gasoline-powered portable drill with a non-magnetic diamond drill bit. These samples were then oriented using a solar and magnetic Pomeroy compass.

They were processed in the Paleomagnetic Laboratory of the Instituto de Astronomia, Geofísica e Ciências Atmosféricas of the University of São Paulo (USPmag, Brazil), where cylindrical cores were prepared in 2.2 cm high standard specimens. After measurement of the natural remanent magnetization (NRM) with a JR-6A spinner magnetometer (AGICO, Czech Republic), stepwise demagnetization was performed to isolate the characteristic remanent magnetization of the specimens (ChRM). We used alternating field (AF) demagnetization up to ~100 mT, using a tumbler Molspin AF demagnetizer, or thermal demagnetization up to ~600 °C, using an ASC TD-48 furnace. For specimens with initial magnetization below 1 $A.m^{-1}$ we used an automated three-axis AF demagnetizer coupled to a horizontal 2G-Enterprises DC-SQUID magnetometer. The ChRM for each specimen was determined using the principal component analysis (PCA) in orthogonal vectors diagrams (Kirschvink, 1980; Zijderveld, 1967), or the intersecting great circle technique (Halls, 1978). Data processing, site mean directions, and paleomagnetic poles were calculated by Fisher's statistics (Fisher, 1953)

Table 1
n/N - number of specimens used in mean directions/number of analyzed specimens; Dec – Declination; Inc – Inclination; R – the resultant vector α95/A95 and k/K - Fisher's statistical parameters (Fisher, 1953) for mean directions and mean virtual geomagnetic poles (VGPs); P.Lat – pole latitude; P.Long – pole longitude. Values of mean sites directions are indicated in bold for positive inclination, negative inclination, and combined polarities. *: underlined/**bold** sites were sampled to attempt baked contact tests. For each site of host rock sampled to attempt a baked contact test, the total number of specimens corresponds to the addition of baked and unbaked samples.

Site (BCT)	Sample	Localization	Thickness	Lithology	Characteristic remanent magnetization (ChRM)						VGP	
					n/N	Dec (°)	Inc (°)	R	k	α95 (°)	P. Lat (°N)	P. Long (°E)
Dykes showing negative inclination												
2	KL02 (A-G)	7.89°S/ 37.08°W	3–4 m	Basalt-andesite	5/8	91	−81.8	*G.C*	*G.C*	10.6	6.4	126.8
4	KL04 (A-G)	7.88°S/ 37.07°W	7.1 m	Basalt-andesite	5/17	301.9	−58.7	*G.C*	*G.C*	12.5	29.4	191.7
5	KL05 (A-G)	7.88°S/ 37.07°W	2.2 m	Basalt-andesite	5/14	292.1	−70.2	*G.C*	*G.C*	8.9	18.5	177.8
6	KL06 (A-G)	7.88°S/ 37.07°W	1.86 m	Basalt-andesite	6/17	271.4	−62	*G.C*	*G.C*	14.1	5.8	190.1
9	KL09 (A-G)	7.88°S/ 37.07°W	8 m	Basalt-andesite	9/15	276.6	−64.4	8.87	61.8	7.1	10.3	187.2
11	KL11 (A-H)	7.68°S/ 36.78°W	2–3 m	Basalt-andesite	7/12	319.4	−51.9	6.71	20.8	13.7	44.9	194
12	KL12 (A-G)	7.68°S/ 36.77°W	2–3 m	Basalt-andesite	8/11	287.6	−65.4	7.88	57.9	7.8	17.5	185.7
13	KL13 (A-F)	7.68°S/ 36.77°W	3–4 m	Basalt-andesite	6/13	259.6	−68.9	*G.C*	*G.C*	10.5	−0.2	180.1
14	KL14 (A-F)	7.88°S/ 37.06°W	4 m	Basalt-andesite	7/10	346.3	−76.1	6.9	60.6	9	32.5	150.2
15	KL15 (A-F)	7.88°S/ 37.06°W	3–4 m	Diorite	12/ 14	136.3	−82.3	11.61	28.4	8.4	−4	132.6
16	KL16 (A-F)	7.88°S/ 37.05°W	1.5 m	Basalt-andesite	5/11	264	−74.2	*G.C*	*G.C*	6.8	3.2	172.4
17	KL17 (A-F)	7.91°S/ 37.03°W	5 m	Basalt-andesite	10/ 12	106.3	−83.8	9.84	57.7	6.7	4.3	131.2
18	KL18 (A-F)	7.92°S/ 37.04°W	3 m	Basalt-andesite	7/13	271.6	−60.5	*G.C*	*G.C*	11	6.4	191.9
19	KL19 (A-F)	7.89°S/ 37.11°W	2 m	Basalt-andesite	7/12	69.2	−86.9	6.81	32.4	10.9	9.2	137.1
Mean dykes (negative inclination)					***14***	***288.8***	***−75.3***	***13.43 12.41***	***22.9 K = 8.2***	***8.5 A95 = 14.8***	***14.3***	***167.5***
1	KL01 (A-G)	7.89°S/ 37.10°W	4 m	Basalt-andesite	5/9	146.8	76.1	4.78	18	19.8	−27.9	339
3	KL03 (A-G)	7.88°S/ 37.07°W	0.75 m	Basalt-andesite	10/ 18	146.7	78.7	*G.C*	*G.C*	12	−24.9	336
7	KL07 (A-G)	7.88°S/ 37.07°W	0.15 m	Basalt-andesite	15/ 20	133.2	55.6	13.91	12.8	11.1	−38.4	11.7
8	KL08 (A-G)	7.88°S/ 37.07°W	5 m	Dolerite	16/ 17	150.9	84	15.75	58.7	4.9	−17.3	329
10	KL10 (A)	7.88°S/ 37.06°W	4 m	Basalt-andesite	5/5	193.6	79.7	4.99	507	3.4	−26.4	317.9
Mean dykes (positive inclination)					***5***	***147***	***75.7***	***4.91 4.79***	***43.1 K = 19***	***11.8 A95 = 18***	***−28.2***	***337.5***
MEAN DYKES COMBINED					***19***	***298.5***	***−76***	***18.29 17.06***	***25.4 K = 9.3***	***6.8 A95 = 11.7***	***−18.2***	***344.9***
Host rocks (baked) - Paleo-mesoproterozoic												
3	KL03 (H-M)	7.88°S/ 37.07°W	Gneiss	Gneiss	12/ 13	137.6	79	11.76	44.9	6.9	−22.3	338.3
4	KL04 (H-N)	7.88°S/ 37.07°W	Gneiss	Gneiss	12/ 17	264.9	−54.5	11.84	67.9	5.4	0.4	197.6
5	KL05 (H-N)	7.88°S/ 37.07°W	Gneiss	Gneiss	7/22	295.3	−72.3	6.77	25.2	14	19.3	174
Mean baked					***3***	***282.6***	***−69.9***	***2.93***	***K = 27.4***	***A95 = 24***	***14.6***	***177.1***
Host rocks (unbaked) - Paleo-mesoproterozoic												
3	KL03 (H-M)	7.88°S/ 37.07°W	Gneiss	Gneiss	1/13	165.1	15.2			12.8	−75.2	52.5
4	KL04 (H-N)	7.88°S/ 37.07°W	Gneiss	Gneiss	5/17	318.2	−0.1	4.71	14	21.2	47.7	240.7
5	KL05 (H-N)	7.88°S/ 37.07°W	Gneiss	Gneiss	15/ 22	307.1	−20.6	14.77	60.6	5	37.8	225.5
6			Gneiss	Gneiss	3/20	311.4	22.1	2.99	187.9	9	37.9	254.2

(*continued on next page*)

Table 1 (*continued*)

Site (BCT)	Sample	Localization	Thickness	Lithology	Characteristic remanent magnetization (ChRM)						VGP	
					n/N	Dec (°)	Inc (°)	R	k	α95 (°)	P. Lat (°N)	P. Long (°E)
	KL06 (H-M)	7.88°S/ 37.07°W										
Mean unbaked					***4***	***320.5***	***−3.7***	***3.71***	***10.3 K = 17.3***	***30 A = 22.8***	***−50.1***	***59.3***

using the PALEOMAC software (Cogné, 2003). GPlates package was used for paleogeographic reconstructions (Boyden et al., 2011).

In addition, magnetic mineralogy of the Monteiro dykes was investigated at the Oceanographic Institute of University of São Paulo, Brazil (IO-USP) to identify the stable remanence carriers. For selected samples we performed hysteresis loops and isothermal remanent magnetization (IRM) using a MicroMag-VSM, Model 3900 (Princeton Measurements Corporation). Thermomagnetic curves (susceptibility versus temperature) were conducted using a CS-4 apparatus coupled to the KLY-4S Kappabridge instrument (AGICO, Brno, Czech. Republic).

4. Paleomagnetic results

Values of natural remanent magnetization for most dykes are of ~0.5–7 A.m^{-1}. with a maximum value of 28.7 A.m^{-1} (KL06C2). A characteristic remanent magnetization (ChRM) was revealed for the Monteiro dykes of northwestern/north direction with a steep negative inclination after removing a secondary component with AF fields above

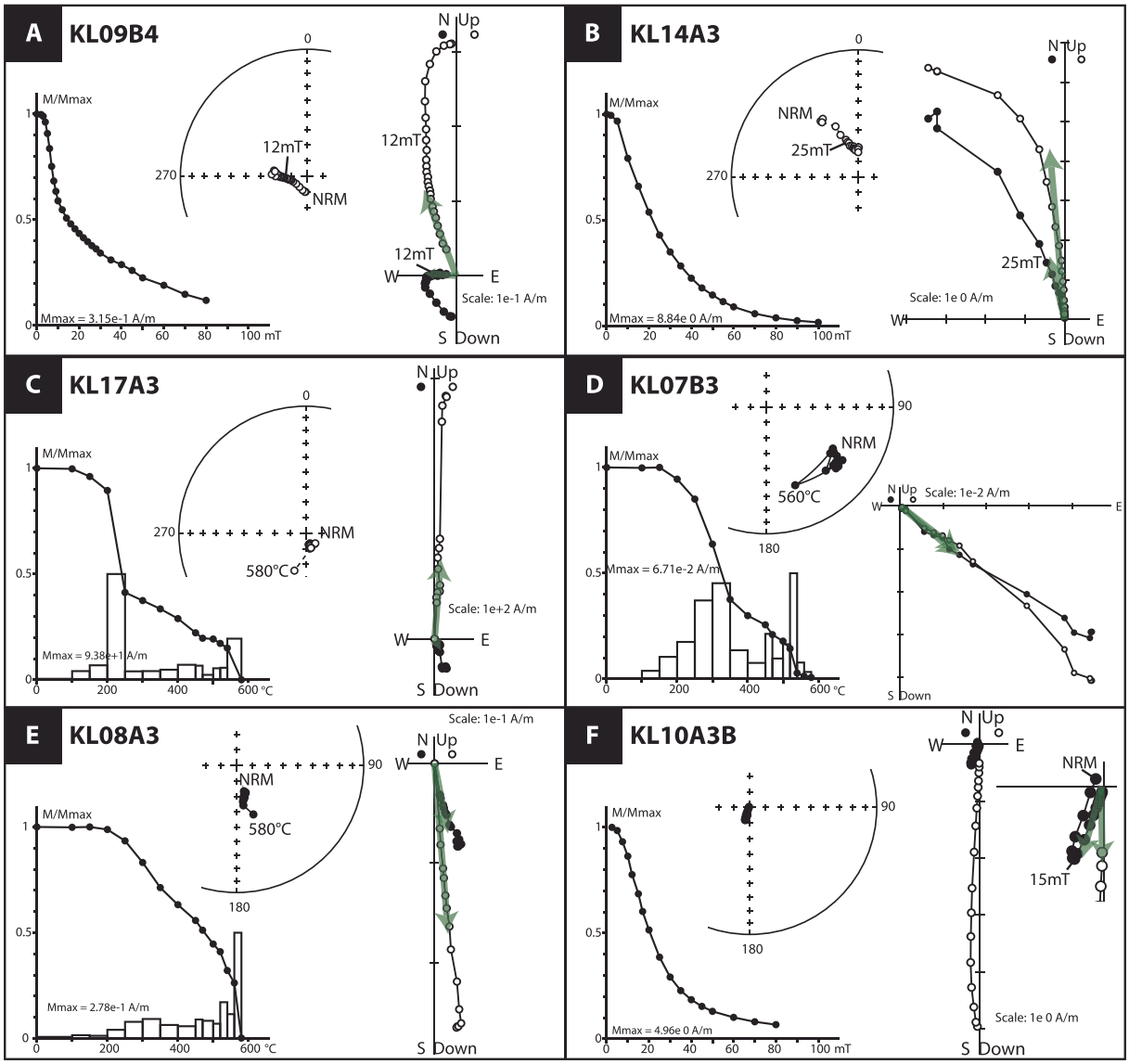

Fig. 3. Representative demagnetization plots of Monteiro dykes for different sites after AF and thermal demagnetizations. Equal-area stereonets (solid (open) symbols represent positive (negative) inclinations) with normalized magnetization intensity curves (M/M_{Max} versus AF amplitude or temperature demagnetization setp), and Zijderveld diagrams (solid (open) symbols represent horizontal (vertical) projections) are presented for each sample.

15 mT (Fig. 3-A-B) and temperatures of ~450–580 °C (Fig. 3-C). Steep positive, southeastern direction were also disclosed for the Monteiro dykes (Fig. 3-D-E-F). Unblocking temperatures (T_{ub}) between 500 and 580 °C indicate magnetite as main carrier of this magnetic component but T_{ub} peak between 250 and 320 °C also suggest the presence of pyrrhotite.

The Monteiro pole (19 sites) was calculated using a combination of 14 dykes with negative directions and 5 dykes with positive directions (Fig. 4). Site KL04 showing a negative direction is well-dated at 538 ± 4 Ma by U-Pb zircon (Hollanda et al., 2010b). Using both negative (Dm = 288.8°, Im = −75.3°, n = 14, k = 22.7) and positive directions (Dm = 147°, Im = 75.7°, n = 5, k = 43.1), the site mean directions is: Dm = 298.5°, Im = −76° (α95 = 6.8°, k = 25.4), and the respective Monteiro paleomagnetic pole is located at 18.2°S and 344.9°E (A95 = 11.7° K = 9.3) (Table 1; Fig. 4-A,B). No VGPs were excluded after using a Vandamme cutoff of 38.8° (Vandamme, 1994), and the VGP dispersion (S value) for the 19 sites is equal to 27° (Fig. 4-B). This relatively high scatter is expected for a high-latitude position considering the statistic paleosecular models of latitudinal dependence of S (*e.g.* Model-G from McFadden et al. (1988)). Moreover, the A95 (~11.7°) is comprised within the A95 envelope (3.7°–12.8°) of Deenen et al. (2011) shown in Fig. 4-B, which means that these results have well-sampled the paleosecular variation. The Monteiro pole passes a reversal test classified as C (McFadden and McElhinny, 1990), with a critical gamma of 15.3° and with an angle between the positive and negative axes of 9.4°.

5. Baked contact tests

Four baked contact tests were attempted to attest the primary magnetization for the Monteiro dykes. A first baked contact test is shown in Fig. 5 for the undated KL05 dyke. The ChRM for the dyke reveal a western direction of high inclination (KL05A3). The thermal demagnetization curve for the dyke's sample shows a high unblocking temperature above 500 °C. A similar direction of high negative inclination is revealed in the sample of host rock at contact (KL05H3). Far away from the contact, a different northwestern direction of lower inclination is observed (KL05K3, KL05L3 samples). All the samples show a high unblocking temperature, but we can observe in this test a decrease in NRM intensity from the contact (1.49 $A.m^{-1}$) as it moves further away (041–0.48 $A.m^{-1}$). As shown by the high unblocking temperature at contact and far away, this field test can be considered as positive. Fig. 6-A shows a schematic representation of a second field test performed for the dated KL04 dyke (7.1 m in width, 538 ± 4 Ma, (Hollanda et al., 2010a)) cross-cutting the Paleoproterozoic basement. Seven cores were sampled in the dyke (A-G) and seven cores in the Paleoproterozoic host rock at the contact (<1 m) and ~14 m away from the contact (Fig. 6-A). Close to the contact (~50 cm), the host rock KL04J3 shows the same characteristic direction of the dyke (*e.g.* specimen KL04C2). The ChRM in this specimen of the host rock was isolated at high temperatures between 500 and 600 °C. At ~9 m from the contact, the specimen KL04L2 also shows the same direction of the dyke. But for samples collected >10 m away from the contact (KL04M and KL04N), the dyke's direction is no longer present in the host rock. At 14 m from the contact, the KL04N3 specimen shows a north/northwestern direction with low inclination. T_{ub} intervals for the characteristic directions isolated from specimen KL04N3 show two peaks at ~300 °C and 530–600 °C with no changes in the magnetic direction. This baked contact test can be considered as positive and shows that the thermal influence of the dyke reached at least ~9 m from the contact for this dyke. Such a distance implies that this test is not purely thermal and suggests a chemical remanent magnetization due to metasomatism in the host rock during the intrusion and cooling (Silva et al., 2006).

Fig. 6-B shows the compilation of site mean directions for each baked contact test performed. For the above KL04 and KL05 baked contact tests, the site mean for baked specimen gives Dm = 264.9°/Im = −54.5° and Dm = 295.3°/Im = −72.3° respectively, which is close to the site mean directions of the corresponding dykes (Dm = 301.9°/Im = −58.7° for KL04 and Dm = 292.1°/Im = −70.2° for KL05) (Table 1; Fig. 6-B). Three baked contact tests (KL03, KL04, KL05) give consistent results in which it was possible to calculate a site mean direction of the baked host

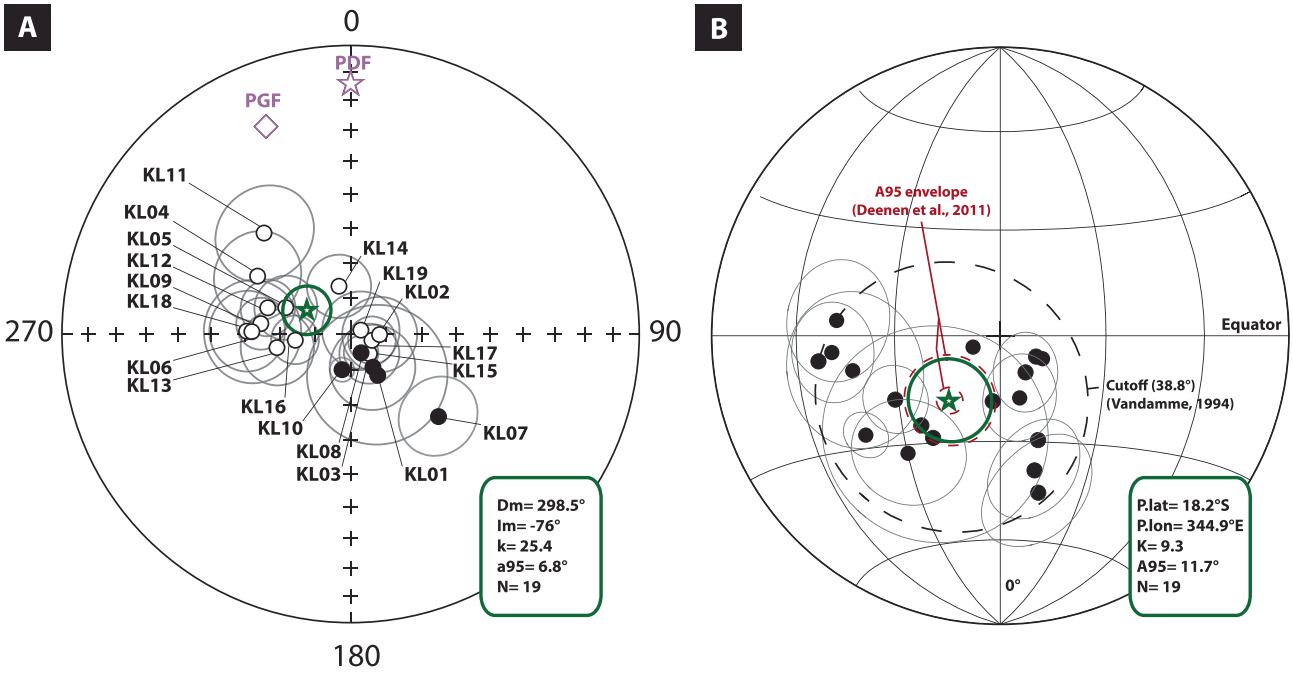

Fig. 4. A: Site mean directions for the Monteiro dykes (in green). Confidence circle (α95) for the calculation of direction of sites and the site mean directions is indicated (Fisher, 1953). Sites with positive and negative directions are represented with full (empty) circles represent downward (upward) inclinations. PDF – Present Dipolar Geomagnetic field; PGF – Present Geomagnetic Field. **B:** Dispersion of site mean virtual geomagnetic poles (VGPs) and paleomagnetic pole calculated for the Monteiro dykes (see Table 1) represented in a Schmidt projection. Statistical parameters A95min (3.7°) and A95max (12.8°) using Deenen et al. (2011) (in red), and the variable cutoff (38.8°) of Vandamme (1994) (in black) are indicated for excluding transitional polarities.

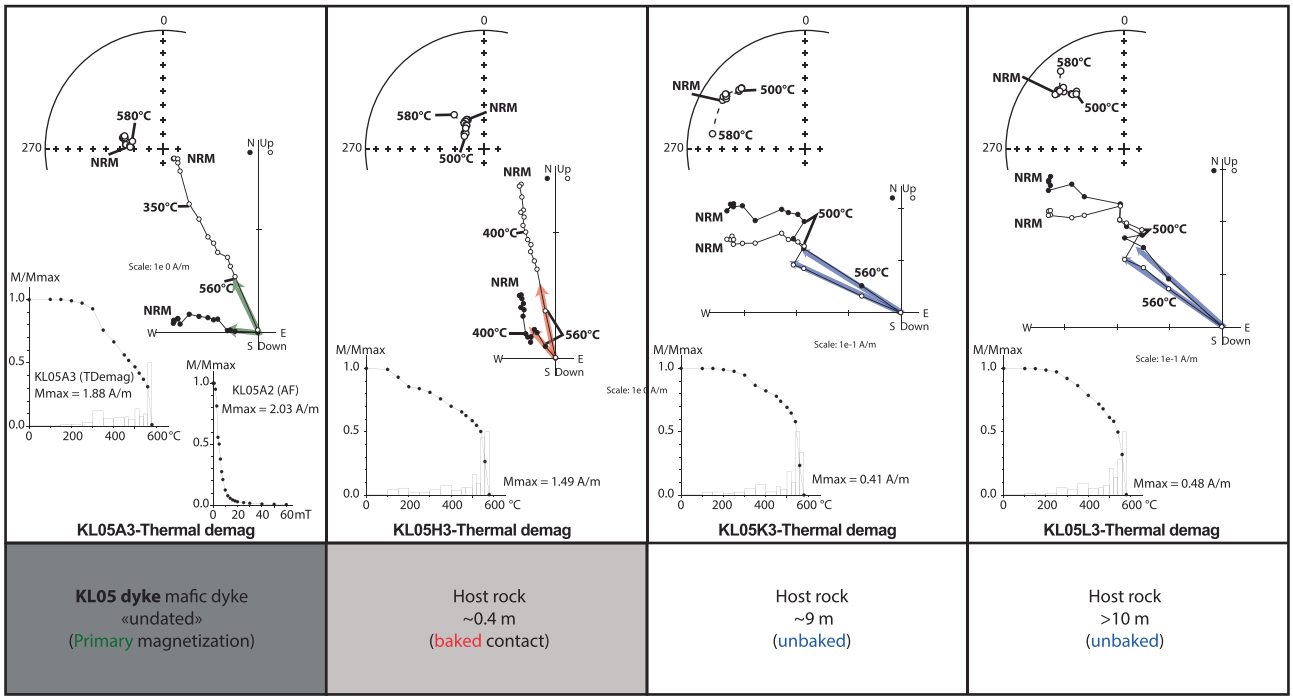

Fig. 5. A: Positive baked contact test (BCT) for the KL05 dyke (undated). AF (KL05A2) and thermal (KL05A3) demagnetization curves are shown for the mafic dyke. The host rock at ~0.4 m (baked, KL05H3) is carrying the same direction than the dyke whereas the host rock samples far away from the contact show a different direction (unbaked, KL03K3 and KL05L3).

rocks showing the dyke's direction (Table 1; Fig. 6-B). As the host rock is a metamorphic rock, the unbaked direction cannot be considered primary. But as shown, the stability of this direction suggests that this magnetization is not a viscous remanent, even if it cannot be definitively discarded because the direction is close to the present field. A complementary study would be necessary to know the age and the origin of the remanence of the host rock, a prerequisite for a high quality contact test (Buchan, 2007a, 2007b). For site KL06 the direction of the host rock close to the contact was unstable therefore this test is considered as negative (see supplementary material – S1l). Overall, the baked contact tests suggest that the direction obtained for the Monteiro dykes is primary and robust to represent the position of the Borborema Province at ~538 Ma.

6. Magnetic mineralogy

From the unblocking temperatures obtained in thermal demagnetizations and the Day's diagram, the magnetic mineralogy for the Monteiro dykes seems to be dominated by SD-PSD (vortex state) magnetite (Fig. 7-A). We note that the samples from the host rock in the baked zone at the KL04 site have a PSD behavior whereas samples collected far from the contact (*e.g.* KL04M1) exhibit a MD behavior which suggests that the contact region was re-heated during the dyke's intrusion and magnetochemical transformations took place in the baked contact (see also D'Agrella-Filho et al. (2004) and Trindade et al. (2006) for similar examples). Magnetic hysteresis for the KL17 sample shows a narrow-waisted behavior typical of SD-PSD magnetite (Fig. 7-B). Its associated IRM curve and Kruiver's decomposition (Kruiver et al., 2001) confirm one dominant phase reaching the saturation with a $B_{1/2}$ value of 24 mT, and presence of a second component of lower contribution with higher coercivity can be associated with a $B_{1/2}$ value of 316 mT (Fig. 7-C). Fig. 7-D shows one example (KL06) for a representative thermomagnetic curve for the Monteiro dykes. The KL06 sample shows a reversible behavior during heating and cooling with a Curie temperature at about 580 °C, which is characteristic of pure magnetite (Fig. 7-D). Presence of pyrrhotite was observed, and hematite was also detected in some altered samples using the thermomagnetic curves.

7. Discussion

7.1. Reliability of the Monteiro paleomagnetic pole (R-criteria)

The Monteiro paleomagnetic pole was calculated using 19 sites of fresh and undeformed fine-grained doleritic to andesitic dykes. This pole satisfies 7 (Q = 7) out the 7 quality criteria proposed by Van der Voo (1990), and satisfies 7 (R = 7) of the recent R-criteria proposed by Meert et al. (2020): **(R1)** The Monteiro dyke swarm is well-dated at 538 ± 4 Ma by SHRIMP U-Pb zircon (site KL04), coeval with the intrusions of Sumé and Santa Catarina plutons (533 ± 4 Ma) in the study area (Hollanda et al., 2010a). These intrusions represent the last pulse of the post-collisional Cariri Magmatic event (~550–530 Ma) during the stabilization of the Borborema Province. **(R2)** Remanence vectors were well-isolated using both stepwise AF treatments and thermal demagnetizations, and processed by the principal component and great circle analyses (Halls, 1978; Kirschvink, 1980) using equal-area projections and Zijderveld diagrams (Zijderveld, 1967). 19 sites and 150 specimens were used to calculate this pole which presents adequate Fisher's statistical parameters (A95 = 11.7° and K = 9.3) (Table 1; Fig. 4). The value of precision K lower than 10, as the limit proposed by Meert et al. (2020), could indicate a weakness of Monteiro results in this criteria, but as indicated this value is purely arbitrary. The statistical method of Deenen et al. (2011), in which Meert et al. (2020) are also based, indicates a superior A95 limit higher than the cone of 95% of confidence A95 of the Monteiro paleomagnetic pole ($A95_{min} = 3.7° < A95_{Monteiro} = 11.7° < A95_{max} = 12.83°$), which shows that these results average the paleosecular variation (Fig. 4). Therefore, we consider that our dataset fulfills all the requirements proposed by Meert et al. (2020) for the R2-criteria. **(R3)** Hysteresis, IRM and thermomagnetic curves show the presence of SD-PSD magnetite as the main carrier of the ChRM (Fig. 7), probably associated to magnetite and ilmenite intergrowths in coarse-grained magnetite grains (Archanjo, 2020). **(R4)** In the shear zone networks of the Borborema Province, strong evidence for a primary

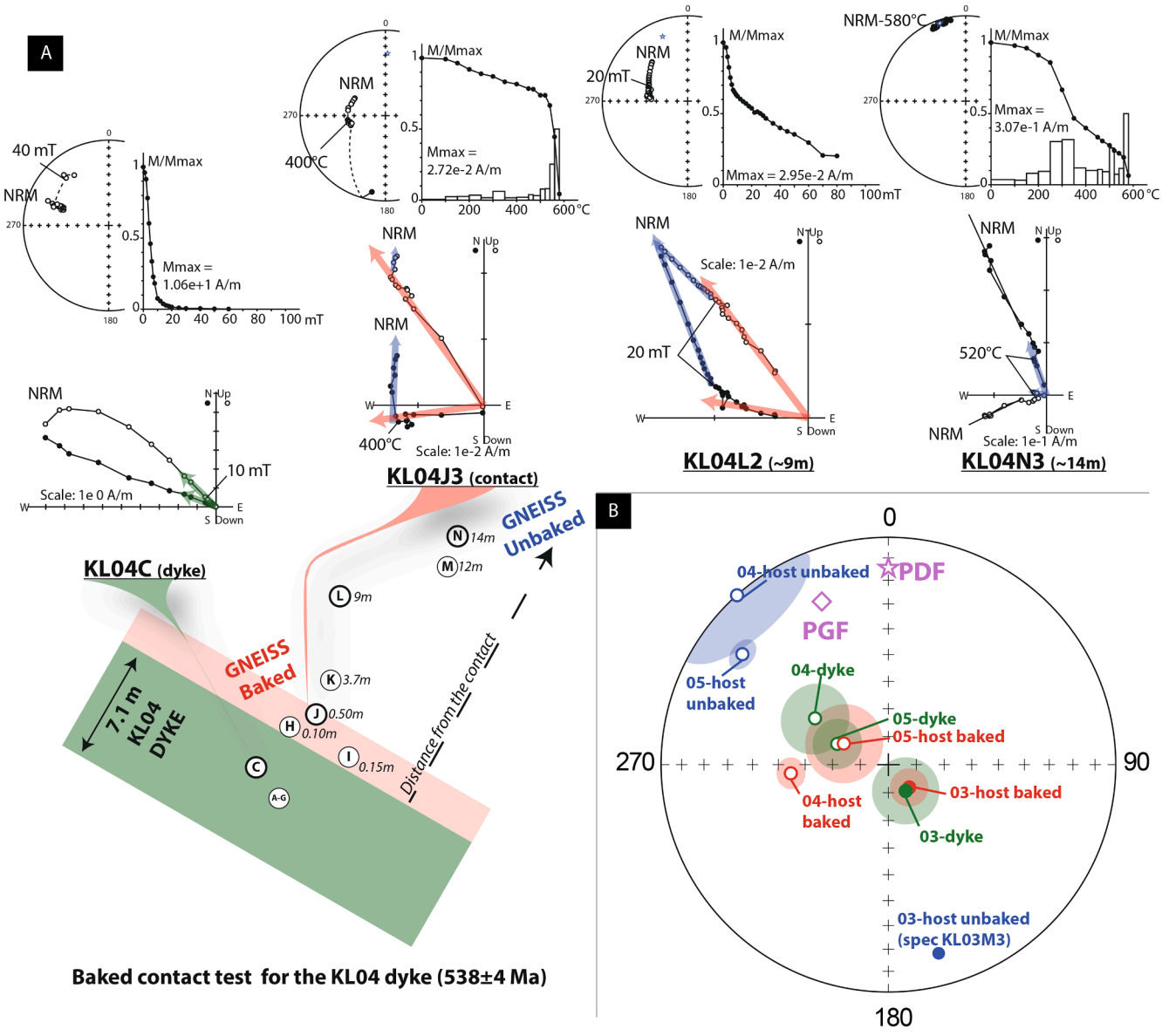

Fig. 6. A: Baked contact test for the KL04 dyke well-dated at 538 ± 4 Ma (Hollanda et al., 2010a). Distance from the contact for each sample is indicated in the cartoon. Demagnetization plots for one sample of the dyke (KL04C2) and different samples of the host rock (KL04J3, KL04L2 and KL04N3) are illustrated. **B:** Site mean directions for three different baked contact tests attempted to prove the primary origin of the magnetization for the Monteiro dykes (Table 1). For each site, a mean site of the host rock was calculated at contact (baked, in red) showing the same direction than the dyke and far away from the contact (unbaked, in blue) showing a different direction. Mean sites with positive and negative directions are represented with full (empty) circles represent downward (upward) inclinations. PDF – Present Dipolar Geomagnetic field; PGF – Present Geomagnetic Field.

remanence is absolutely required. A positive baked contact test was shown in this study for three sites (KL03, KL04, KL05) which suggest a regional stability for the host rock direction away from dyke margins. These baked contact tests prove that the isolated direction for the Monteiro dykes was acquired during the intrusion and cooling of these mafic intrusions at ~538 Ma. (**R5**) The study area is surrounded by shear zones with the Coxixola SZ in the North and the Congo SZ in South (Fig. 1). Ar-Ar muscovite cooling ages for mylonites of East Coxixola SZ indicate plateau ages of ~548–546 Ma showing that the area was already cold the dykes intruded (Hollanda et al., 2010a). Latter localized reactivation of these shear zones was possible until ~513 Ma, but these younger ages can also reflect the different cooling histories along the shear zone (Hollanda et al., 2010a). Anisotropy of magnetic susceptibility (AMS) data for the plutons in this area indicate an emplacement within a slight clockwise rotation from Santa Catarina to Sumé in agreement with the presence of the dextral Coxixola shear zone, but these data discard any large displacement along the shear zones (Hollanda et al., 2010a). The angular distance of 57° between the ~540 Ma Monteiro pole (SF1, Fig. 8B) and the ~520 Ma Itabaiana dykes (SF2, Fig. 8B) (Trindade et al., 2006) is not compatible with any realistic large tectonic displacement (>5000 km) within this same tectonic province and should be addressed as a drift issue. Furthermore, a vertical-axis tectonic rotation is also excluded between these two key poles because it would involve extreme rotations (>140°). Despite a possible localized reactivation of the shear zones, the study area has not undergone significant deformation between 540 and 520 Ma and fulfills the R5-criteria. (**R6**) The ~538 Ma Monteiro pole passes the reversal test (R_c) with 14 negative and 5 positive polarities. (**R7**) The Monteiro pole is different from the robust poles calculated for younger units in the Borborema Province or the São Francisco craton (Tohver et al., 2006). We can thus consider the ~538 Ma Monteiro paleomagnetic pole as a key pole (R = 7) according to the definition of Buchan (2013).

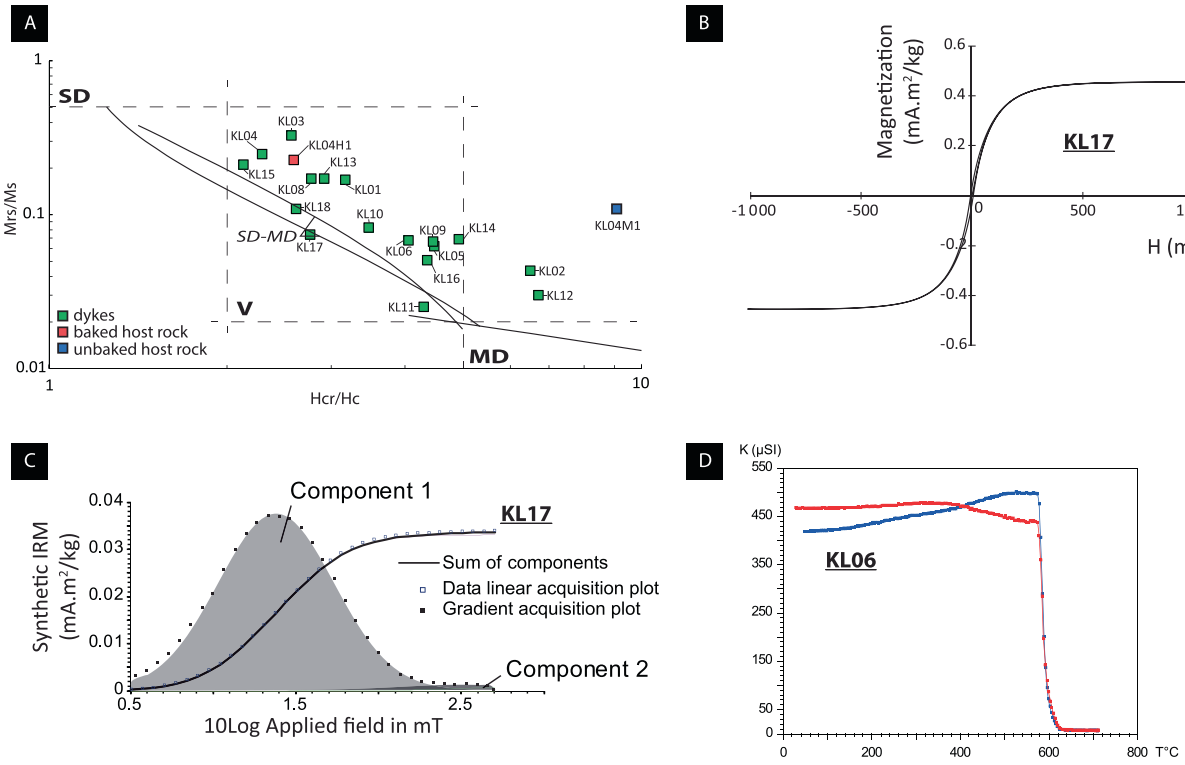

Fig. 7. A: Day plot for samples of the Monteiro dykes (in green), and for two host rock samples (KL04H1, baked in red, and KL04M1, unbaked in blue). **B:** Representative hysteresis loop corrected of paramagnetic contribution (sample KL17). **C:** IRM decomposition of Kruiver et al. (2001) for the KL17 sample. **D:** Example of a thermomagnetic curve for the KL06 sample.

7.2. Classical apparent polar wander paths of Gondwana

The assembly of Gondwana during the Ediacaran-Cambrian times was considered a long process involving many orogens (Meert and Lieberman, 2008; Schmitt et al., 2018). Paleomagnetism is the only method to provide quantitative information on the latitude and paleo-orientation of the continents and is essential to produce paleogeographical reconstruction considering all the geological information available during the period of interest (Besse et al., 2011). Between ~620 and 500 Ma, the available paleomagnetic database for the Gondwana is composed of various poles from Australia, East Antarctica, Amazonia, São Francisco, Congo, Madagascar, and West Africa. Hence, several apparent polar wander paths (APWPs) have been proposed for Gondwana (McElhinny et al., 2003; Meert et al., 2001; Meert, 2003; Merdith et al., 2017; Mitchell et al., 2010, 2011; Rapalini, 2018; Robert et al., 2017; Tohver et al., 2006; Trindade et al., 2006).

In the "tight fit" Gondwana frame (Reeves et al., 2004; Trindade et al., 2006), the apparent polar wander path (APWP) shows a long curve from a south polar position at ~595 Ma to an equatorial cluster of poles at ~525–510 Ma, named hereafter as the RTT curve proposed by Rapalini (2018), Tohver et al. (2006), and Trindade et al. (2006) (Table 2 for the database; Fig. 8-A-B). This APW path implies a latitudinal drift (~24–31 cm/yr) of Gondwana from an equatorial position to a polar position in this Ediacaran-Cambrian interval (~595–510 Ma) (Trindade et al., 2006).

The poles located in the south polar position of the curve at ~595–575 Ma are essentially from the Rio de la Plata craton with Playa Hermosa Formation (RP1) (Rapalini et al., 2015), Vila Mónica Formation (RP2) (Rapalini et al., 2013), Cerro Largo Formation. (RP3) (Rapalini et al., 2013), Barrientos claystones (RP4) (Rapalini, 2006), and the key Sierra de las Animas Complex (RP6) (Rapalini et al., 2015) (Fig. 8-B). The last pole on the curve is from the Luis Alves block with the volcanic Campo Alegre Formation (LA1) (D'Agrella-Filho and Pacca, 1988). A pole from the Arabian Nubian Shield was also determined at ~593 Ma for the Dokhan volcanics (AR1) but its position is slightly different of the curve with the possibility of an independent history before joining the NE Gondwana (Nairn et al., 1987) (Fig. 8-C). We added to the RTT curve, two robust poles of ~571 Ma (R ~ 6) recently available for Africa, comprising the Nola metadolerite (P1) from Central African Republic, and the C component of Adrar-n-takoucht volcanics (AF2) from Morocco (Robert et al., 2017) (Fig. 8-C). It is worth noting that in this ~595–570 Ma interval, only the Sierra de las Animas Complex pole (Rapalini et al., 2015) fulfills the seven R-criteria of quality (Meert et al., 2020). Four poles were available in the interval 560–535 Ma for the western Gondwana according to Rapalini (2018) - the Sinyai metadolerite (P2) (Meert and Van Der Voo, 1996), the Mirbat sediments (AR2) (Kempf et al., 2000), the Olavarría Formation (RP5) (Rapalini et al., 2013), and the Cerro Negro Formation (RP7) (Rapalini et al., 2013). Completing the updated RTT curve, two poles of the eastern Gondwana were used in the 560–535 Ma interval, comprising the ~545 Ma Upper Arumbera (A8) (Kirschvink, 1978), and the ~535 Ma Hawker group (A9) (Klootwijk, 1980) (Fig. 8-D).

The younger portion of the APW path of Gondwana between ~530 and 500 Ma contrasts with its longer older portion and is in mid-equatorial latitudes between 0° and 40°N (Fig. 8). This time interval is represented by all the continents and start with the ~525 Ma Itabaiana key pole (R = 7) of the Borborema Province which defines the northwestern part of the curve (Trindade et al., 2006) (Fig. 8-B). For the Amazonia craton, the ~525 Puga B carbonate pole (Trindade et al., 2003) is close to the ~525 Ma Itabaiana pole but failed a fold test and is considered a remagnetization at ~525 Ma according to its position on the APW path (Tohver et al., 2010; Trindade and Amaral, 2017). The poles of São Francisco Bambui B (SF3) and the Bambui-Salitre C (SF4) are also regarded as a remagnetization at ~525–520 Ma (Trindade et al., 2004). They are followed by two metamorphic poles, the Juiz de Fora Complex (SF5) (D'Agrella-Filho et al., 2004) and the Piquete Formation (SF6) (D'Agrella Filho et al., 1986), with the magnetization interval estimated at ~510–500 Ma. For West Africa, it worth noting that the

~507 Ma Sidi-Said Maachou volcanics (AF5) is anomalous even though a baked contact test is available (El Attari et al., 2019; Khattach et al., 1995) (Fig. 8-C). Two metamorphic poles were determined in Madagascar with the Madagascar virgation zone (MA1) (Meert et al., 2003) and the Carion granite (MA2) (Meert et al., 2001) well-dated by Ar-Ar to constrain the magnetization age at 521 ± 12 Ma and 512.7 ± 1.3 Ma, respectively. Two others metamorphic poles for the Pan-African belts complete this dataset with the remagnetization of the Equeefa dykes and Mzumbe gneiss (P3) at ~530 Ma (Gose et al., 2004), and the Ntonya Ring pole (P4) estimated at ~522 Ma (Briden, 1968). The new ~514 Ma Campanario Formation for the Pampia terrane (Pa1) is also consistent with this APW path (Franceschinis et al., 2020). For Australia and East Antarctica, the paleomagnetic poles between ~520 and 500 Ma are relatively well-clustered and consistent with the ~520–500 Ma portion of the APW path of Gondwana (see Table 2 and Fig. 8-D). Trindade et al. (2006) proposed a "Z-shape" APW path curve between ~525 Ma and 500 Ma using the tight-fit configuration for Gondwana (Reeves et al., 2004) to explain this paleomagnetic poles distribution.

Among the major paleogeographical implications of the RTT curve, the Rio de la Plata must already have joined the Congo-São Francisco at

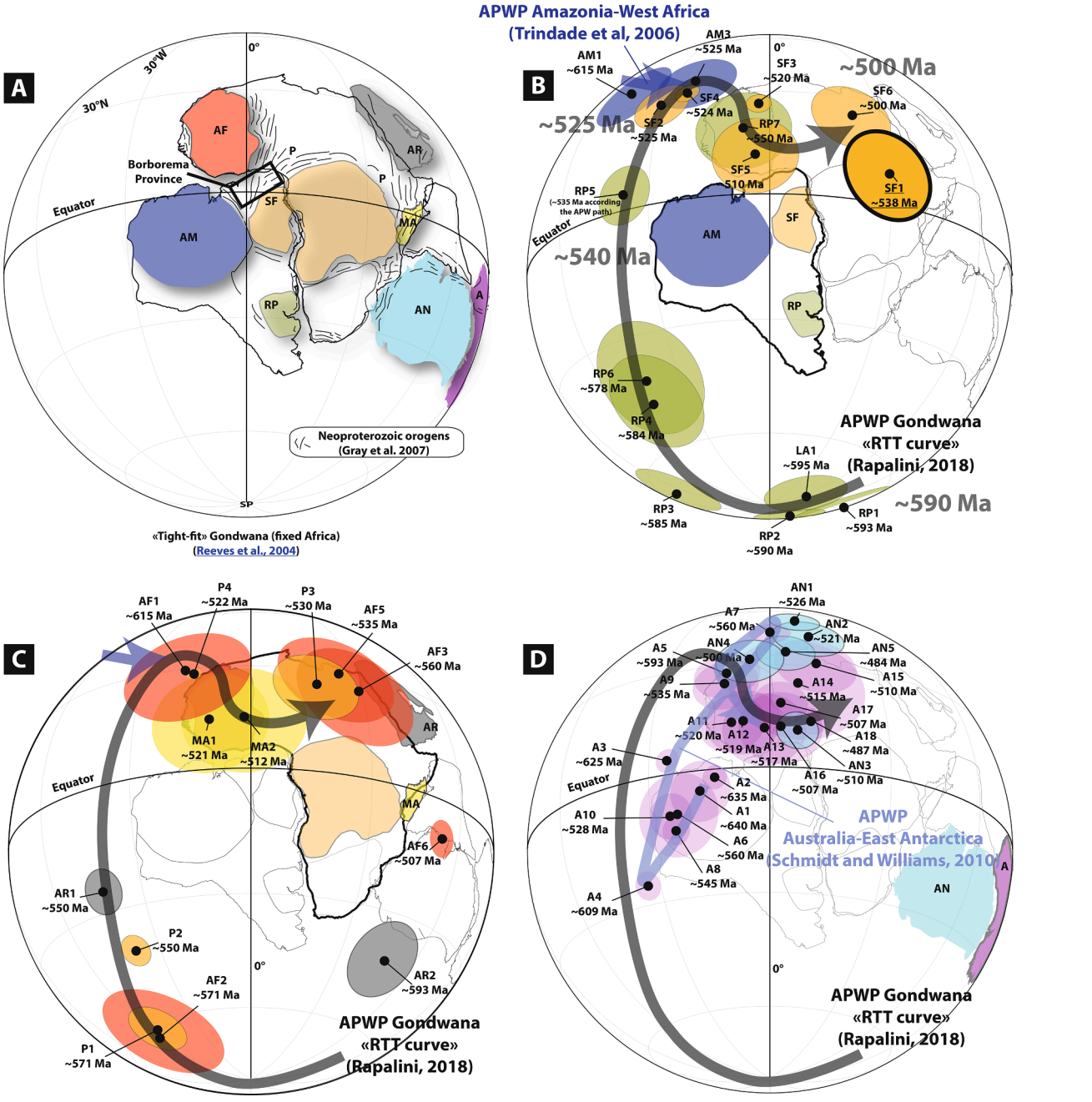

Fig. 8. Classical apparent polar wander path (APWP) for the Gondwana (RTT curve) (Rapalini, 2018; Tohver et al., 2006; Trindade et al., 2006). **A:** "Tigh-fit" Gondwana reconstruction in the African frame (Reeves et al., 2004; Trindade et al., 2006). *Abbreviations for cratonic units and associated paleomagnetic poles*: AM – Amazonia (blue), AF – West Africa (red), SF – São Francisco-Congo (brown), RP – Rio de la Plata (light green), AR – Arabian Nubian Shield (grey), MA – Madagascar (yellow), AN – Antarctica (blue), A – Australia (purple), P – Pan-African Belts (black). Position of the Borborema Province is indicated. Neoproterozoic orogens are indicated according to Gray et al. (2007). **B:** APW path for the South American cratons. **C:** APW path for African units, Arabian Nubian Shield, and Madagascar. **D:** APW for Eastern Gondwana (Australia and East Antarctica) according to Schmidt and Williams (2010). Classical APW path for the Gondwana is indicated (Rapalini, 2018; Tohver et al., 2006; Trindade et al., 2006).

Table 2

Paleomagnetic database for the Gondwana. S.lat – site latitude, S.lon – site longitude, Dec – declination, Inc – inclination, k, α95, A95, Fisher's statistics of mean directions and paleomagnetic poles, Plat – pole latitude, Plon – Pole longitude, Age – nominal age used in the paleogeographical reconstructions. Q-criteria (Van der Voo, 1990). *References:* **Australia:** (Embleton and Giddings, 1974; Kirschvink, 1978; Klootwijk, 1980; Mitchell et al., 2010; Schmidt et al., 1993, 2009; Schmidt and Williams, 1996, 2010; Sohl et al., 1999; Williams, 2008). **East Antarctica:** (Encarnación and Grunow, 1996; Funaki, 1984; Grunow and Encarnación, 2000; Manzoni and Nanni, 1977; Zijderveld, 1968). **Rio de la Plata:** (D'Agrella-Filho and Pacca, 1988; Rapalini, 2006; Rapalini et al., 2013, 2015). **São Francisco-Borborema:** (D'Agrella-Filho et al., 2004; D'Agrella Filho et al., 1986; Trindade et al., 2004, 2006). **Amazonia craton:** (D'Agrella Filho et al., 2018; Garcia et al., 2013; Trindade et al., 2003; Trindade and Amaral, 2017). **West Africa:** (Khattach et al., 1995; Morel, 1981; Robert et al., 2017). **Pan-African Belts:** (Briden, 1968; Gose et al., 2004; Meert and Van Der Voo, 1996; Moloto-A-Kenguemba et al., 2008). **Arabian Nubian Shield:** (Kempf et al., 2000; Kilner et al., 2005; Nairn et al., 1987). **Madagascar:** (Meert et al., 2001, 2003).

Code	Name	Lithology	S.lat	S.lon	Dec	Inc	k	α95	A_{95} (dp/dm)	Plat (°N)	Plong (°E)	Age (Ma)	1	2	3	4	5	6	7	Q	References
AUSTRALIA																					
A18	Black Hill Norite	Intr	−34.4	139	231.1	19.7	67.5	3.8	3/6	−37.5	34.4	487	X	X	X	0	X	0	X	**5**	Schmidt et al. (1993)
A17	Lower L. Frome	Sedi	−31	140	232.3	−0.5	16.6	10.1	5.1/10.1	−31.4	26.9	507	X	X	X	0	X	X	X	**6**	Klootwijk (1980)
A16	Giles Creek	Sedi	−23.62	134.49	227.5	−9	5	32.6	10	−38	25	507	X	X	X	0	X	X	X	**6**	Klootwijk (1980)
A15	Hugh River shale, Jay Creek limestone	Sedi	−23.8	133.2	234.8	2.2	6.1	26.6	10	−19.3	39.1	510	X	X	X	0	X	X	X	**6**	Mitchell et al. (2010)
A14	Aroona Dam sediments	Sedi	−30.61	138.35	213	5	8.5	15.1	16.5	−26	33	515	X	0	0	0	0	X	X	**3**	Embleton and Giddings (1974)
A13	Billy Creek Fm	Sedi	−31	140	224.1	−1.2	11	14.4	7.2/14.4	−37.4	20.1	517	X	X	X	0	X	X	X	**6**	Klootwijk (1980)
A12	Kangaroo Is red	Sedi	−36	138	224.5	−4.4	9.4	12.3	6.2/12.3	−33.8	15.1	519	X	X	X	0	X	X	X	**6**	Klootwijk (1980)
A11	Pertaoorta Group	Sedi	−31	140	258	20.5	18	29.9	8	−33	12	520	X	X	X	0	X	X	X	**6**	Klootwijk (1980)
A10	Todd River Dolomite	Sedi	−23.6	134.5	19.3	35	14.7	6.7	4.5/7.7	−43.2	339.9	528	X	X	X	X	X	0	X	**6**	Kirschvink (1978)
A9	Hawker Group	Sedi	−32	138.5	233.4	−27.8	12.3	11	6.8/12.5	−21.3	14.9	535	X	X	X	0	X	X	X	**6**	Klootwijk (1980)
A8	Arumbera sandstone (Upper)	Sedi	−23.6	134.5	16.2	31.2	22.6	4.1	3.5	−46.6	337.4	545	X	X	X	X	X	X	X	**7**	Kirschvink (1978)
A7	Wonoka Fm	Sedi	−32	138.5	255.9	−23.7	8.1	6.4	3.6/6.8	−5.2	30.5	560	0	X	X	X	X	X	X	**6**	Schmidt and Williams (2010)
A6	Arumbera (Lower), Pertatataka Fm. (Upper)	Sedi	−23.6	134.5	20.2	32.4	14	12	10.2	−44.3	341.9	560	X	X	X	X	X	X	X	**7**	Kirschvink (1978)
A5	Bunyeroo Fm	Sedi	−32	138.5	56.6	29.3	40.4	10.7	6.5/11.8	−18.1	16.3	593	0	X	X	X	X	X	0	**5**	Schmidt and Williams (1996)
A4	Brachina Fm	Sedi	−32	138.5	178.2	−22.6	12.4	4.4	2.4/4.6	−46.0	315.4	609	0	X	X	X	X	X	X	**6**	Schmidt and Williams (2010)
A3	Nuccaleena Fm	Sedi	−31.6	138.8	208.3	−34.9	13.1	3.4	2.2/3.9	−32.3	350.8	625	0	X	X	X	X	X	X	**6**	Schmidt et al. (2009)
A2	Elatina Fm	Sedi	−32	138.5	208.3	−12.9	9.9	4.2	2.1/4.2	−43.7	359.3	635	0	X	X	X	X	X	X	**6**	Schmidt et al. (2009), Williams (2008)
A1	Yaltipena Fm	Sedi	−32	138.5	204	−16.4	12.2	11	5.9/11.4	−44.2	352.7	640	0	X	X	X	X	X	X	**6**	Sohl et al. (1999)
EAST ANTARCTICA																					
AN5	Lamprophyre dykes, Taylor Valley	Intr	−77.64	163.35	222.6	0.6		10.6	7	−9.3	26.7	484	X	X	X	0	0	0	X	**4**	Manzoni and Nanni (1977)
AN4	Granitic rocks, Wright Valley	Intr	−77.516	161.66	216.7	−9		8.1	8.1	−5.4	18.5	500	0	X	X	X	0	0	X	**4**	Funaki (1984)
AN3	Sor Rondane intrusions (Queen Maud Mountains)	Intr	−72	24	341.5	64		4.5	5	−29	10	510	X	0	X	0	0	0	X	**3**	Zijderveld (1968)
AN2	Zanuck granite	Intr	−86.2	−150	183.8	7.2	23.7	10.8	8.6	−7.3	36.2	521	X	X	X	0	0	X	0	**4**	Grunow and Encarnación (2000)
AN1	Wyatt Ackerman Mt. Paine tonalite	Intr	−86.2	−150	189.3	−9	34.7	7.9	6	1.3	39.8	526	X	X	X	0	0	X	X	**5**	Grunow and Encarnación (2000); Encarnación and Grunow (1996)

(*continued on next page*)

Table 2 (*continued*)

Code	Name	Lithology	S.lat	S.lon	Dec	Inc	k	α95	A_{95} (dp/dm)	Plat (°N)	Plong (°E)	Age (Ma)	1	2	3	4	5	6	7	Q	References
SOUTH AMERICA																					
Rio de la Plata craton - Luis Alves block																					
RP7	Cerro Negro Formation (CN)	Sedi	−37.3	−59.2	28.7	56.1	15	9.5	11.5	11.8	323	550	X	0	X	X	X	X	0	**5**	Rapalini et al. (2013)
RP6	Sierra de las Animas Complex (SA)	Intr	−34.6	−55.3	108	−60.6	20	10.4	14.9	−12.2	258.9	578	X	X	X	X	X	X	X	**7**	Rapalini et al. (2015)
RP5	Olavarría Fm (OL)	Sedi	−37.3	−59.2	349.3	49.9	37	7	7.5	21.7	289.9	580	0	0	X	0	X	0	0	**2**	Rapalini et al. (2013)
RP4	Los Barrientos claystones (LB)	Sedi	−37.8	−59	104.5	60.8	23	9.3	12.9	−16.2	253.9	585	0	X	X	X	X	X	X	**6**	Rapalini (2006)
RP3	Cerro Largo Fm (CL)	Sedi	−37.3	−59.2	73.7	−36.6	15	12.1	11	−24.8	217.4	585	0	0	X	0	X	0	X	**3**	Rapalini et al. (2013)
RP2	Villa Mónica Fm (VM)	Sedi	−37.3	−59.2	43.4	−36.3	45	9.1	8.5	−48.8	198.1	590	0	0	X	0	X	0	X	**3**	Rapalini et al. (2013)
RP1	Playa Hermosa Formation (PH)	Sedi	−34	−55.5	207.6	27.3		12.4	12.1	−58.8	183.1	593	X	0	X	0	X	0	X	**4**	Rapalini et al. (2015)
LA1	Campo Alegre Formation (Luis Alves block)	Intr	−26.5	−49.3	36	−40	56	10	9	−57	223	595	X	X	X	0	X	X	X	**6**	D'Agrella-Filho and Pacca (1988)
São Francisco craton - Borborema Province																					
SF6	Piquete Formation (Ribeira Belt)	Metam	−21.5	−42.5	60	68		10	10	−1	347	500	0	X	X	0	X	0	0	**3**	D'Agrella Filho et al. (1986)
SF5	Juiz de fora complex (Ribeira Belt)	Metam	−21.5	−42.5	2.9	75.4	17.9	6.4	10.3	4.2	320.1	510	0	X	X	0	X	0	0	**3**	D'Agrella-Filho et al. (2004)
SF4	Bambui + Salitre C (remag)	Sedi	−12.5	−41	5.8	63.2	105.1	2.9	3	32	322	525	1	X	X	1	X	0	0	**3**	Trindade et al. (2004)
SF3	Bambui B	Sedi	−12.5	−41	25.6	68.3	247.5	1.6	3	15	331	520	2	X	X	2	X	0	0	**3**	Trindade et al. (2004)
SF2	Itabaiana dykes	Intr	−7.2	−35.5	168	−64	46	5.7	7.3	34.9	314.6	525	X	X	X	X	X	X	X	**7**	Trindade et al. (2006)
SF1	Monteiro dykes	Intr	−7.8	−37.06	298.5	−76	25.4	6.8	11.7	−18.2	344.9	538	X	X	X	X	X	X	X	**7**	**This study**
Amazonia craton																					
AM3	Puga B (Araras Group) (remag)	Sedi	−16	−58	25.7	55.4	28.9	7	10	34	327	525	0	X	X	−1	0	X	X	**3**	Trindade et al. (2003)
AM2	Puga A (Araras Group) (remag)	Sedi							9	83	113	630	0	X	X	−1	0	X	X	**3**	Trindade et al. (2003), Trindade and Amaral (2017)
AM1	Planalto da Serra	Intr	−14.5	−54.5	7.2	46.1	24.35	10	10.8	49.7	313.4	615	X	X	X	0	X	0	X	**5**	Garcia et al. (2013), D'Agrella Filho et al. (2018)
AFRICA																					
West Africa																					
AF6	Sidi-Said-Maachou Volc.	Extr	33.1	−8.1	300	−31	70	6	4.5	−14	51	507	X	X	X	X	X	0	X	**6**	Khattach et al. (1995)
AF5	Djebel Boho Volc. (B2)	Extr	30.3	−7.5	87.7	71.9	14.9	9.9	14.9	27.3	27.1	535	X	X	X	X	X	X	X	**7**	Robert et al. (2017)
AF4	Ouarzazate Volc.(A)	Extr							4.1	−29.3	56.6	0	0	X	X	0	0	0	0	**2**	Robert et al. (2017)
AF3	Fajjoud and Tagougast Volc. (B1)	Extr	30.3	−7.5	93.7	67	10.7	10.5	15.6	21.9	31	560	X	X	X	X	X	0	X	**6**	Robert et al. (2017)
AF2	Adrar-n-takoucht Volc. (C-comp)	Extr	30.3	−7.5	26.6	18.2	7.4	20.4	15.7	−57.6	295.6	571	X	X	X	0	0	X	X	**5**	Robert et al. (2017)
AF1	Adma diorite	Intr	18.3	1.2	317.3	78.6	22	9	15.9	32.5	344.7	615	X	X	X	0	X	0	X	**5**	Morel (1981)

(*continued on next page*)

Table 2 (*continued*)

Code	Name	Lithology	S.lat	S.lon	Dec	Inc	k	α95	A_{95} (dp/dm)	Plat (°N)	Plong (°E)	Age (Ma)	1	2	3	4	5	6	7	Q	References
Pan-African Belts																					
P4	Ntonya Ring	Metam	−15.2	35.2	311.3	42.8	1054	1.9	1.8	28	345	522	X	X	X	0	X	0	0	4	Briden (1968)
P3	Equeefa dykes and Mzumbe gneiss	Metam	−30.5	30.5	346.5	51.4	32.7	9.8	10.6	24.7	17.4	530	0	X	X	0	0	0	0	2	Gose et al. (2004)
P2	Sinyai Metadolerite	Metam	0.2	37.05	241	20	20	5	3/5	−29	319	550	X	X	X	0	X	X	0	5	Meert and Van der Voo (1996)
P1	Nola Metadolerite	Metam	3.5	16	26.7	−11.2	24.01	10.5	5/10	−61.8	304.8	571	X	X	X	0	X	X	X	6	Moloto-A-Kenguemba et al. (2008)
Arabian Nubian Shield																					
AR3	Mirbat sediments	Sedi	17.05	54.46	69.5	18.5	46.4	7.2	3.9/7.5	−23.3	321.8	~550	0	0	X	0	X	0	X	3	Kempf et al. (2000)
AR2	Mirbat + Huqf	Sedi	17.05	54.46					7.3	−52.3	74.4	600	0	X	X	X	X	X	X	6	Kilner et al. (2005)
AR1	Dokhan volcanics (Egypt)	Intr	26.6	33.6	178.1	36.8	33.3	9.64	10	−42.7	36.2	593	0	X	X	0	0	0	X	3	Nairn et al. (1987)
Madagascar																					
MA2	Carion granite	Metam	−18.7	47.5	278	62	27	11	13/17	−6.8	1	512	X	X	X	0	X	X	X	6	Meert et al. (2001)
MA1	Madagascar virgation zone	Metam	−18.5	47.3	271	54	14.4	10.1	14.2	−6.7	352.6	521	X	X	X	0	X	X	X	6	Meert et al. (2003)

~580 Ma and the APW path implies a fast drift during the last phases of Gondwana assembly (Rapalini, 2018). The Arabian Nubian Shield was near or associated to the northeastern part of Gondwana at ~550 Ma and the amalgamation of the Eastern Gondwana (Australia and the East Antarctica) occurred later in Cambrian times (Rapalini, 2018; Schmidt, 2014). The APW path of Amazonia-West Africa since ~620 Ma is distinct from the Gondwana APW with the ~615 Ma Planalto da Serra pole (AM1) (D'Agrella Filho et al., 2018; Garcia et al., 2013) for Amazonia close to the ~610 Ma Adma diorite pole (AF1) (Morel, 1981) for West Africa which support a connection with Laurentia at ~615 Ma (Trindade et al., 2006). Their later subsequent separation from Laurentia and amalgamation into Gondwana is poorly constrained by the current paleomagnetic database (Tohver et al., 2006; Trindade et al., 2006). A singularity of this paleomagnetic model is the possibility of a large Ediacaran Clymene Ocean between Amazonia and São Francisco-Congo plus Rio de la Plata cratons (Cordani et al., 2013b; Tohver et al., 2010, 2012; Tohver and Trindade, 2014; Trindade et al., 2006).

Our new high-quality ~538 Ma Monteiro paleomagnetic pole (SF1) does not fit the ~540–530 Ma APW path of the classical RTT curve (Fig. 8-B). This interval is poorly constrained in the RTT curve by only one low-quality paleomagnetic pole, the Olavarría Formation (RP5) (Rapalini et al., 2013). RP5 pole is not well-defined (R = 1) and its age was estimated according its position on the RTT curve by interpolation. Thus, RP5 cannot be considered as robust to define the APW path. Moreover, a robust estimation of ~600–590 Ma was recently proposed for the Olavarría Formation - RP5 pole (Gómez-Peral et al., 2019). Therefore, no more pole constrains the RTT curve for the Western Gondwana in the 570–525 Ma interval. Recently, two robust paleomagnetic poles were obtained for West Africa with the Fajjoud and Tagougast volcanics B1 (AF3), and the ~535 Ma Djebel Boho volcanics B2 (AF5) (Robert et al., 2017). These poles do not fit the RTT curve either, but oddly, our new ~538 Ma Monteiro pole is consistent with the ~535 Ma AF5 pole (Fig. 8-C) suggesting a different APW for the Gondwana.

7.3. IITPW and rapid oscillations of the APWP of Gondwana during the Ediacarian-Cambrian.

Based on three new paleomagnetic poles obtained for West Africa (AF2, AF3, AF5) (Robert et al., 2017) and the position of the ~615 Ma Adma diorite (AF1) (Morel, 1981), Robert et al. (2017) suggested a different APW path for West Africa (Fig. 9-A), which is generally associated to Amazonia (D'Agrella-Filho et al., 2016). Their hypothesis is consistent with the position of the ~615 Ma Planalto da Serra pole (AM1) (D'Agrella Filho et al., 2018; Garcia et al., 2013) for Amazonia, not considered by Robert et al. (2017) (Fig. 9-A). This new APW path is composed of two large paleomagnetic shifts of ~90° with the first between ~615–571 Ma and the second between ~571–565 Ma (Robert et al., 2017) (Fig. 9-A). Moreover, a large oscillation was also proposed by Mitchell et al. (2010) for Gondwana on the basis of poles from Australia and East Antarctica and also based on discordant poles of Laurentia and Baltica (Robert et al., 2017). This worldwide oscillation (Creveling et al., 2012) with ~90° amplitude is consistent with an inertial interchange true polar wander (IITPW) (Goldreich and Toomre, 1969; Kirschvink et al., 1997; Rose and Buffett, 2017).

The position of the key ~538 Ma Monteiro pole for the Borborema Province (SF1) is consistent with the end of the oscillation proposed by Robert et al. (2017) and the position of the coeval ~535 Ma Djebel Boho B2 pole (Robert et al., 2017) which gives a strong support for this APW path (Fig. 9-A). This large IITPW is also supported by the position of the RP5 pole using the new estimation of ~600–590 Ma for the Olavarría Fm. (RP5 pole) (Gómez-Peral et al., 2019). Following this large IITPW, the Cambrian APW path of Gondwana produce equatorial rapid and small oscillations between ~538 Ma and 500 Ma, with a first shift between ~540 and 525 Ma not compatible with the normal, Phanerozoic-like lithospheric plates velocity (Fig. 9-B). Therefore, it seems that these

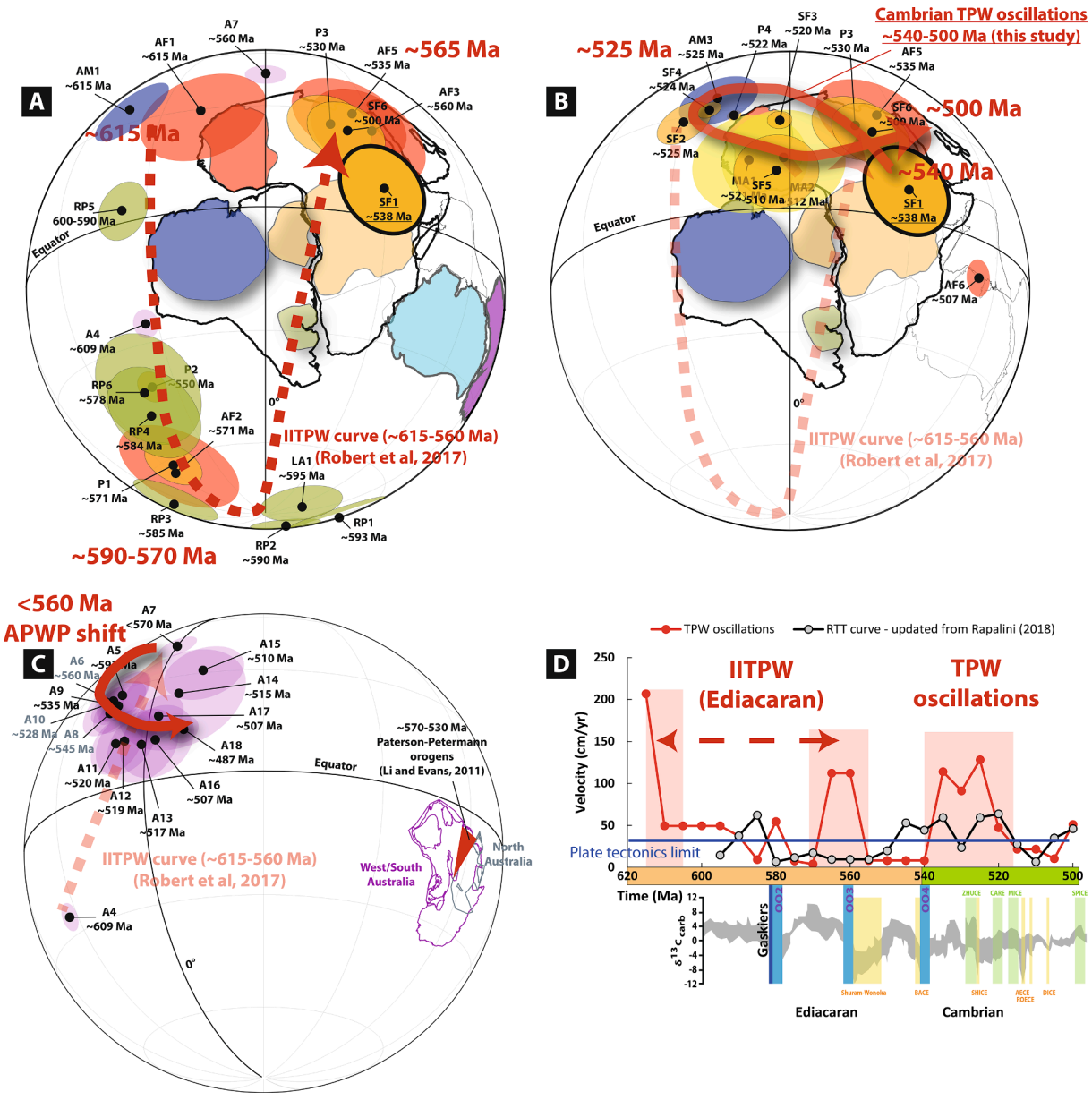

Fig. 9. **A:** Inertial interchange true polar wander (IITPW) between ~615 and 560 Ma for the Gondwanan poles according to the curve from Robert et al. (2017). Position of the key ~538 Ma Monteiro paleomagnetic pole (SF1) is indicated. **B:** Cambrian TPW oscillations of the between ~540 and 500 Ma as suggested in this study. **C:** Paleomagnetic poles of Australia showing a large dispersion between ~609 and 560 Ma (Robert et al., 2017) and an counterclockwise motion after 560 Ma until ~500 Ma. **D:** Comparison of magnitude velocity (cm/yr) for the Gondwana between the RTT curve (in black) and the Ediacaran IITPW - CambrianTPW oscillations curve (in red). Velocity data were obtained using a time interval of 5 Ma (available in supplementary material – S2). Plate tectonics limit of ~30 cm/yr is indicated (Meert et al., 1993). Ediacaran C-isotope compilation ($\delta^{13}C_{carb}$) with indication for the Carbon isotope excursions (yellow-negative and green-positive) modified from Wood et al. (2019). *Abbreviations*: ZHUCE, Zhujiaqing; CARE, Cambrian arthropod radiation; SHICE, Shiyantou; MICE, Mingxinsi; AECE, Archaeocyath Extinction; ROECE, Redlichiid-Olenellid Extinction; DICE, Drumian. Position of the ~580 Ma Gaskiers glaciation is indicated. Estimation for episodic oceanic oxygenation events (OOE) from Sahoo et al. (2016).

oscillations do not end at ~560 Ma as proposed by Robert et al. (2017), but the proposed APW path in this study reflects a more complex pattern of TPW rapid oscillations spanning the Cambrian period (Fig. 9-B), which reconciles some previous observations (Jiao et al., 2018; Kirschvink et al., 1997; Mitchell et al., 2010, 2011). Comparison with the paleomagnetic data of Eastern Gondwana is more delicate because no high-quality poles are available for Eastern Antarctica (the paleohorizontal is not constrained) and the poles for Australia between 640 and 500 Ma are only obtained from sedimentary units. We followed the APW path of Robert et al. (2017) corrected of the Ediacarian-Cambrian ~40° counterclockwise rotation between North and South Australia cratons along the Patterson-Petermann orogens (570–530 Ma) (Li and Evans, 2011). After the ~610–560 Ma IITPW, no oscillations are observed for the poorly-defined ~540–500 Ma interval of Australia, maybe because of superimposed plate motion or lack of high-quality data (Fig. 9-C).

The updated RTT curve of the Gondwana APW path suggests a high velocity above ~50 cm/yr at ~590 Ma and a rapid shift after 550 Ma (Fig. 9-D). In our refined APW path, the two shifts of the IITPW are visible with velocities above ~100 cm/yr, and the position of the ~538 Ma Monteiro pole (this study) implies also high velocities at ~540 Ma not compatible with the ~30 cm/yr plate tectonics speed limit (Meert et al., 1993).

We can speculate about the origin of these small oscillations: (1) these rapid oscillations after a large IITPW may be a coincidence, but

they are perpendicular to the latter and related to the assembly of the large continental landmass of Gondwana between ~550 and 500 Ma (Robert et al., 2018; Schmitt et al., 2018). These events can also be correlated with the development of the ~615–540 Ma Central Iapetus Magmatic Province (CIMP) (Youbi et al., 2020). The CIMP is related to the emplacement of a mantle plume in polar position preceding the opening of the Iapetus Ocean between Laurentia, Baltica, and Amazonia (Robert et al., 2020). Cambrian oscillations were also recently proposed by Jiao et al. (2018) for South China between the Lower-Middle and Upper Cambrian sequences (~505–500 Ma) but the lower sequence is lacking evidence for primary magnetization. These poles from South China are not considered in this work due to the still poor constraints on the precise configuration of South China in Gondwana. In order to support these TPW oscillations, new high-quality paleomagnetic poles are needed in this interval for major cratons like Laurentia, Baltica, and Siberia; (2) they can also represent small and rapid motions of the Gondwana landmass after complete assembly; (3) alternatively, we cannot exclude the possibility of the existence of a weakened dipole with frequent reversals through the Cambrian to explain this anomalous paleomagnetic behavior (Bazhenov et al., 2016; Gallet et al., 2019; Meert et al., 2016).

Any attempt at correlation between the Ediacaran-Cambrian major events, as the rise of oxygen and the Cambrian radiation (~540–520 Ma), with the existence of true polar wander events may seem fortuitous due the quality of data and the lack of geochronological on these events. A link with global geodynamics that affects environmental conditions cannot be completely ruled out. Mitchell et al. (2015) suggested that TPW can increase the net diversity according to the latitudinal diversity gradient during the latitudinal variations (LDG-TPW model) and that these TPW are associated to the Cambrian radiation. Interesting, this carbon excursion behavior corresponds to our TPW oscillations period between ~540 and 510 Ma (Fig. 9-D) where we observed curious excursions in the APW path of the Gondwana. Changes in latitudes during TPW events can result in dramatic changes in ocean continental patterns and sea level influencing the geochemical cycles (Kirschvink and Raub, 2003; Mound and Mitrovica, 1998; Mound et al., 1999; Raub et al., 2007).

8. Conclusions

To refine the APW path for the Gondwana in the Ediacaran-Cambrian interval, we carried out a detailed paleomagnetic study from the ~538 Ma Monteiro dyke swarm. 19 sites give a new high-quality paleomagnetic pole (R = 7) located at 18.2°S and 344.9°E (A95 = 11.7° K = 9.3). The magnetic mineralogy indicates that PSD magnetite is the main carrier of the remanence and its primary origin is supported by three baked contact tests. This key pole passes a reversal test using 14 sites with negative inclinations and 5 sites with positive inclinations. Moreover, the VGP's dispersion suggests that the paleosecular variation was removed. This new pole of reference for the Ediacaran-Cambrian transition indicates a directional shift in the APW path of the Gondwana after the end of an inertial interchange true polar wander (IITPW) at ~560 Ma. Using the compilation of paleomagnetic poles available for the Gondwana, this study suggests rapid and small oscillations of the APW path during the Cambrian (~540–510 Ma). These rapid oscillations are strangely concomitant with short-lived carbon excursions and episodic oceanic oxygenation events during the Cambrian. A fortuitous link between these TPWs and global changes in biochemical cycles cannot be dismissed.

CRediT authorship contribution statement

Paul Yves Jean Antonio: Investigation, Conceptualization, Visualization, Writing - original draft. **Ricardo Ivan Ferreira Trindade:** Project administration, Methodology, Supervision, Funding acquisition, Investigation, Writing - review & editing. **Bruno Giacomini:** Investigation, Methodology, Formal analysis. **Daniele Brandt:** Investigation, Validation, Writing - review & editing. **Eric Tohver:** Investigation.

Declaration of Competing Interest

The authors declare that they have no known competing financial interests or personal relationships that could have appeared to influence the work reported in this paper.

Acknowledgements

We thank the Brazilian Fundação de Amparo à Pesquisa do Estado de São Paulo (FAPESP grants 2017/18840-6, 2018/23755-0) and funding of the associated thematic project (2016/06114-6). We thank the "Centro Oceanografico de Registros Estratigraficos (CORE), Insituto Oceanografico da Univerdade de São Paulo" for VSM using. We thank Maria Helena Hollanda to point out these dykes and for her help with field information. We would like to thank the editor M. Schannor and two reviewers (L. Gallo and one anonymous) for their constructive comments and suggestions to improve the quality of this paper.

Appendix A. Supplementary data

Supplementary data to this article can be found online at https://doi.org/10.1016/j.precamres.2021.106243.

References

Abrajevitch, A., Van der Voo, R., 2010. Incompatible Ediacaran paleomagnetic directions suggest an equatorial geomagnetic dipole hypothesis. Earth Planet. Sci. Lett. 293, 164–170.
Almeida, F.F.M., Hasui, Y., Neves, B.B.D., Fuck, R.A., 1981. Brazilian Structural Provinces: an Introduction. Earth Sci. Rev. 17, 1–29.
Archanjo, C.J., Hollanda, M.H.B.M., Rodrigues, S.W.O., Neves, B.B.B., Armstrong, R., 2008. Fabrics of pre- and syntectonic granite plutons and chronology of shear zones in the Eastern Borborema Province, NE Brazil. J. Struct. Geol. 30, 310–326.
Archanjo, C.J., 2020. Composite magmatic/magnetic fabrics evidences late AMS in syntectonic dikes in the Monteiro-Sumé plutonic-volcanic complex (NE Brazil). J. Struct. Geol. 140, 104–154.
Arthaud, M.H., Caby, R., Fuck, R.A., Dantas, E.L., Parente, C.V., 2008. Geology of the northern Borborema Province, NE Brazil and its correlation with Nigeria, NW Africa. Geol. Soc., London, Spec. Publ. 294, 49–67.
Bazhenov, M.L., Levashova, N.M., Meert, J.G., Golovanova, I.V., Danukalov, K.N., Fedorova, N.M., 2016. Late Ediacaran magnetostratigraphy of Baltica: evidence for Magnetic Field Hyperactivity? Earth Planet. Sci. Lett. 435, 124–135.
Besse, J., Courtillot, V., Greff, M., 2011. Paleomagnetism, polar wander. In: Gupta, H.K. (Ed.), Encyclopedia of Solid Earth Geophysics. Springer, Netherlands, Dordrecht, pp. 945–955.
Bono, R.K., Tarduno, J.A., 2015. A stable Ediacaran Earth recorded by single silicate crystals of the ca. 565 Ma Sept-Îles intrusion. Geology 43, 131–134.
Bono, R.K., Tarduno, J.A., Nimmo, F., Cottrell, R.D., 2019. Young inner core inferred from Ediacaran ultra-low geomagnetic field intensity. Nat. Geosci. 12, 143.
Boyden, J.A., Müller, R.D., Gurnis, M., Torsvik, T.H., Clark, J.A., Turner, M., Ivey-Law, H., Watson, R.J., Cannon, J.S., 2011. Next-generation plate-tectonic reconstructions using GPlates. In: Geoinformatics: Cyberinfrastructure for the Solid Earth Sciences, pp. 95–114.
Briden, J.C., 1968. Paleomagnetism of the Ntonya Ring Structure, Malawi. J. Geophys. Res. 1896–1977 (73), 725–733.
Brito Neves, B.B.D., Santos, E.D., Van Schmus, W.R., 2000. Tectonic history of the Borborema Province. Tectonic Evol. South Am. 31, 15.
Buchan, K.L., Ernst, R.E., Hamilton, M.A., Mertanen, S., Pesonen, L.J., Elming, S.-Å., 2001. Rodinia: the evidence from integrated palaeomagnetism and U-Pb geochronology. Precambr. Res. 110, 9–32.
Buchan, K.L., 2007a. Baked contact test. In: Encyclopedia of Geomagnetism and Paleomagnetism. Springer, pp. 35–39.
Buchan, K.L., 2007b. Pole, key paleomagnetic. In: Encyclopedia of Geomagnetism and Paleomagnetism. Springer, pp. 839–840.
Buchan, K.L., 2013. Key paleomagnetic poles and their use in Proterozoic continent and supercontinent reconstructions: a review. Precambr. Res. 238, 93–110.
Caby, R., Sial, A., Arthaud, M., Vauchez, A., 1990. Crustal evolution and the brasiliano orogeny in Northeast Brazil, 2012. In: Dallmeyer, R.D., Lécorché, J.P. (Eds.), The West African orogens and circum-Atlantic correlatives. Springer Science & Business Media, pp. 373–397 (2012).
Cawood, P.A., Pisarevsky, S.A., 2017. Laurentia-Baltica-Amazonia relations during Rodinia assembly. Precambr. Res. 292, 386–397.

Cogné, J.P., 2003. PaleoMac: a Macintosh™ application for treating paleomagnetic data and making plate reconstructions. Geochem. Geophys. Geosyst. 4, 1007.
Cordani, U.G., Pimentel, M.M., de Araújo, C.E.G., Fuck, R.A., 2013a. The significance of the Transbrasiliano-Kandi tectonic corridor for the amalgamation of West Gondwana. Braz. J. Geol. 43, 583–597.
Cordani, U.G., Pimentel, M.M., Ganade De Araújo, C.E., Basei, M.A.S., Fuck, R.A., Girardi, V.A.V., 2013b. Was there an Ediacaran Clymene Ocean in central South America? Am. J. Sci. 313, 517–539.
Creveling, J.R., Mitrovica, J.X., Chan, N.H., Latychev, K., Matsuyama, I., 2012. Mechanisms for oscillatory true polar wander. Nature 491, 244–248.
D'Agrella-Filho, M.S., Raposo, M.I.B., Egydio-Silva, M., 2004. Paleomagnetic study of the Juiz de Fora Complex, SE Brazil: implications for Gondwana. Gondwana Res. 7, 103–113.
D'Agrella-Filho, M., Pacca, I., 1988. Palaeomagnetism of the Itajai, Castro and Bom Jardim groups from southern Brazil. Geophys. J. Int. 93, 365–376.
D'Agrella Filho, M., Pacca, I., Sato, K., 1986. Paleomagnetism of Metamorphic Rocks from de Piquete Region-Ribeira Valley, Southeastern Brazil. Rev. Bras. Geof. 4, 79–84.
D'Agrella Filho, M.S., Trindade, R.I.F., Garcia, M.S.R., Ruiz, A.S., Bispo-Santos, F., Hollanda, M.H., 2018. The Planalto da Serra Alkaline-rock Complex: new 40Ar/39Ar ages and paleomagnetic results, and implications for the Gondwana formation. In: South American Symposium on Isotope Geology, 11th SSAGI, Cochabamba, Bolivia, p. 71.
D'Agrella-Filho, M.S., Pacca, I.I.G., Trindade, R.I.F., Teixeira, W., Raposo, M.I.B., Onstott, T.C., 2004. Paleomagnetism and 40Ar/39Ar ages of mafic dikes from Salvador (Brazil): new constraints on the São Francisco craton APW path between 1080 and 1010 Ma. Precambr. Res. 132, 55–77.
D'Agrella-Filho, M.S., Bispo-Santos, F., Trindade, R.I.F., Antonio, P.Y.J., 2016. Paleomagnetism of the Amazonian Craton and its role in paleocontinents. Braz. J. Geol. 46, 275–299.
Dalziel, I.W.D., 1997. OVERVIEW: Neoproterozoic-Paleozoic geography and tectonics: review, hypothesis, environmental speculation. Geol. Soc. Am. Bull. 109, 16–42.
Dantas, E., Cawood, P., Lages, G., Lima, H., Santos, E., Caxito, F., 2019. Early to late Neoproterozoic subduction-accretion episodes in the Cariris Velhos Belt of the Borborema Province, Brazil: Insights from isotope and whole-rock geochemical data of supracrustal and granitic rocks. J. S. Am. Earth Sci. 102384.
Davison, I., Dos Santos, R.A., 1989. Tectonic evolution of the Sergipano Fold Belt, NE Brazil, during the Brasiliano orogeny. Precambr. Res. 45, 319–342.
de Wit, M.J., Stankiewicz, J., Reeves, C., 2008. Restoring Pan-African-Brasiliano connections: more Gondwana control, less Trans-Atlantic corruption. Geol. Soc., London, Spec. Publ. 294, 399–412.
Deenen, M.H.L., Langereis, C.G., van Hinsbergen, D.J.J., Biggin, A.J., 2011. Geomagnetic secular variation and the statistics of palaeomagnetic directions. Geophys. J. Int. 186, 509–520.
dos Santos, E.J., Schmus, W.R.V., Kozuch, M., Neves, B.B.D.B., 2010. The Cariris Velhos tectonic event in Northeast Brazil. J. S. Am. Earth Sci. 29, 61–76.
Driscoll, P.E., Evans, D.A.D., 2016. Frequency of Proterozoic geomagnetic superchrons. Earth Planet. Sci. Lett. 437, 9–14.
Duan, Z., Liu, Q., Ren, S., Li, L., Deng, X., Liu, J., 2018. Magnetic reversal frequency in the Lower Cambrian Niutitang Formation, Hunan Province, South China. Geophys. J. Int. 214, 1301–1312.
El Attari, A., Pereira, M.F., Ezzouhairi, H., El Houicha, M., Jouhari, A., Berrada, I., Fekkak, A., Ennih, N., Hoepffner, C.H., Gama, C., Silva, J.B., 2019. Zircon U-Pb geochronology and geochemistry of Cambrian magmatism in the Coastal Block (Oued Rhebar volcanic complex, Moroccan Meseta): implications for the geodynamic evolutionary model of North-Gondwana. J. Afr. Earth Sc. 160, 103598.
Embleton, B.J.J., Giddings, J.W., 1974. Late Precambrian and Lower Palaeozoic palaeomagnetic results from South Australia and Western Australia. Earth Planet. Sci. Lett. 22, 355–365.
Encarnación, J., Grunow, A., 1996. Changing magmatic and tectonic styles along the paleo-Pacific margin of Gondwana and the onset of early Paleozoic magmatism in Antarctica. Tectonics 15, 1325–1341.
Fisher, R., 1953. Dispersion on a Sphere. Proc. R. Soc. London. Ser. A. Math. Phys. Sci. 217, 295–305.
Franceschinis, P.R., Rapalini, A.E., Escayola, M.P., Rodríguez Piceda, C., 2020. Paleogeographic and tectonic evolution of the Pampia Terrane in the Cambrian: new paleomagnetic constraints. Tectonophysics 779, 228386.
Funaki, M., 1984. Investigation of the paleomagnetism of the basement complex of Wright Valley, Southern Victoria Land, Antarctica. J. Geomagn. Geoelec. 36, 529–563.
Gallet, Y., Pavlov, V., Courtillot, V., 2003. Magnetic reversal frequency and apparent polar wander of the Siberian platform in the earliest Palaeozoic, inferred from the Khorbusuonka river section (northeastern Siberia). Geophys. J. Int. 154, 829–840.
Gallet, Y., Pavlov, V.E., 2016. Three distinct reversing modes in the geodynamo. Izv. Phys. Solid Earth 52, 291–296.
Gallet, Y., Pavlov, V., Korovnikov, I., 2019. Extreme geomagnetic reversal frequency during the Middle Cambrian as revealed by the magnetostratigraphy of the Khorbusuonka section (northeastern Siberia). Earth Planet. Sci. Lett. 528, 115823.
Ganade, C.E., Cordani, U.G., Agbossoumounde, Y., Caby, R., Basei, M.A.S., Weinberg, R. F., Sato, K., 2016. Tightening-up NE Brazil and NW Africa connections: New U-Pb/Lu–Hf zircon data of a complete plate tectonic cycle in the Dahomey belt of the West Gondwana Orogen in Togo and Benin. Precambr. Res. 276, 24–42.
Ganade de Araujo, C.E., Rubatto, D., Hermann, J., Cordani, U.G., Caby, R., Basei, M.A.S., 2014a. Ediacaran 2,500-km-long synchronous deep continental subduction in the West Gondwana Orogen. Nat. Commun. 5, 5198.
Ganade de Araujo, C.E., Weinberg, R.F., Cordani, U.G., 2014b. Extruding the Borborema Province (NE-Brazil): a two-stage Neoproterozoic collision process. Terra Nova 26, 157–168.
Garcia, M.S., Trindade, R.I., Manoel, S., Pinho, F.E., 2013. Paleomagnetismo do complexo alcalino Planalto da Serra (Mato Grosso): Implicações para a formação do Gondwana, In: Letters, L. (Ed.), Latinmag Letters, Montevideo, pp. OB19, 11-18.
Goldreich, P., Toomre, A., 1969. Some remarks on polar wandering. J. Geophys. Res. 74, 2555–2567.
Gómez-Peral, L.E., Arrouy, M.J., Poiré, D.G., Cavarozzi, C.E., 2019. Redox-sensitive trace element distribution in the Loma Negra Formation in Argentina: the record of an Ediacaran oxygenation event. Precambr. Res. 332, 105384.
Gose, W.A., Johnston, S.T., Thomas, R.J., 2004. Age of magnetization of Mesoproterozoic rocks from the Natal sector of the Namaqua-Natal belt, South Africa. J. Afr. Earth Sci. 40, 137–145.
Gray, D.R., Foster, D.A., Maas, R., Spaggiari, C.V., Gregory, R.T., Goscombe, B., Hoffmann, K., 2007. Continental growth and recycling by accretion of deformed turbidite fans and remnant ocean basins: examples from Neoproterozoic and Phanerozoic orogens. Mem. –Geol. Soc. Am. 200, 63.
Grunow, A.M., Encarnación, J., 2000. Terranes or Cambrian polar wander: New data from the Scott Glacier area, Transantarctic Mountains, Antarctica. Tectonics 19, 168–181.
Halls, H.C., 1978. The use of converging remagnetization circles in palaeomagnetism. Phys. Earth Planet. Inter. 16, 1–11.
Hoffman, P.F., 1991. Did the breakout of Laurentia turn Gondwanaland inside-out? Science 252, 1409.
Hoffman, P.F., Schrag, D.P., 2002. The snowball Earth hypothesis: testing the limits of global change. Terra Nova 14, 129–155.
Hollanda, M.H.B.M., Archanjo, C.J., Souza, L.C., Armstrong, R., Vas,, 2010a. Cambrian mafic to felsic magmatism and its connections with transcurrent shear zones of the Borborema Province (NE Brazil): Implications for the late assembly of the West Gondwana. Precambr. Res. 178, 1–14.
Hollanda, M.H.B.M., Archanjo, C.J., Souza, L.C., Armstrong, R., Vasconcelos, P.M., 2010b. Cambrian mafic to felsic magmatism and its connections with transcurrent shear zones of the Borborema Province (NE Brazil): implications for the late assembly of the West Gondwana. Precambr. Res. 178, 1–14.
Jiao, W.-J., Li, Y.-X., Yang, Z.-Y., 2018. Paleomagnetism of a well-dated marine succession in South China: a possible Late Cambrian true polar wander (TPW). Phys. Earth Planet. Inter. 277, 38–54.
Kempf, O., Kellerhals, P., Lowrie, W., Matter, A., 2000. Paleomagnetic directions in Late Precambrian glaciomarine sediments of the Mirbat Sandstone Formation, Oman. Earth Planet. Sci. Lett. 175, 181–190.
Khattach, D., Robardet, M., Perroud, H., 1995. A Cambrian pole for the Moroccan Coastal Meseta. Geophys. J. Int. 120, 132–144.
Kilner, B., Niocaill, C., Brasier, M., 2005. Low-latitude glaciation in the Neoproterozoic of Oman. Geology 33, 413–416.
Kirschvink, J., 1978. The Precambrian-Cambrian boundary problem: paleomagnetic directions from the Amadeus Basin, central Australia. Earth Planet. Sci. Lett. 40, 91–100.
Kirschvink, J.L., 1980. The least-squares line and plane and the analysis of palaeomagnetic data. Geophys. J. Int. 62, 699–718.
Kirschvink, J.L., 1992. Late Proterozoic low-latitude global glaciation: the snowball Earth. 51-52.
Kirschvink, J.L., Ripperdan, R.L., Evans, D.A., 1997. Evidence for a Large-Scale Reorganization of Early Cambrian Continental Masses by Inertial Interchange True Polar Wander. Science 277, 541–545.
Kirschvink, J.L., Raub, T.D., 2003. A methane fuse for the Cambrian explosion: carbon cycles and true polar wander. C.R. Geosci. 335, 65–78.
Klootwijk, C.T., 1980. Early palaeozoic palaeomagnetism in Australia I. Cambrian results from the Flinders Ranges, South Australia II. Late Early Cambrian results from Kangaroo Island, South Australia III. Middle to early-Late Cambrian results from the Amadeus Basin, Northern Territory. Tectonophysics 64, 249–332.
Knoll, A.H., 1992. The early evolution of eukaryotes: a geological perspective. Science 256, 622.
Kruiver, P.P., Dekkers, M.J., Heslop, D., 2001. Quantification of magnetic coercivity components by the analysis of acquisition curves of isothermal remanent magnetisation. Earth Planet. Sci. Lett. 189, 269–276.
Landeau, M., Aubert, J., Olson, P., 2017. The signature of inner-core nucleation on the geodynamo. Earth Planet. Sci. Lett. 465, 193–204.
Lhuillier, F., Hulot, G., Gallet, Y., Schwaiger, T., 2019. Impact of inner-core size on the dipole field behaviour of numerical dynamo simulations. Geophys. J. Int. 218, 179–189.
Li, Z.-X., Evans, D.A.D., 2011. Late Neoproterozoic 40° intraplate rotation within Australia allows for a tighter-fitting and longer-lasting Rodinia. Geology 39, 39–42.
Manzoni, M., Nanni, T., 1977. Paleomagnetism of ordovician lamprophyres from Taylor Valley, Victoria Land, Antarctica. Pure Appl. Geophys. 115, 961–977.
McElhinny, M.W., Powell, C.M., Pisarevsky, S.A., 2003. Paleozoic terranes of eastern Australia and the drift history of Gondwana. Tectonophysics 362, 41–65.
McFadden, P.L., Merrill, R.T., McElhinny, M.W., 1988. Dipole/quadrupole family modeling of paleosecular variation. J. Geophys. Res. Solid Earth 93, 11583–11588.
McFadden, P.L., McElhinny, M.W., 1990. Classification of the reversal test in palaeomagnetism. Geophys. J. Int. 103, 725–729.
Meert, J.G., Voo, R.V.D., Powell, C.M., Li, Z.-X., McElhinny, M.W., Chen, Z., Symons, D. T.A., 1993. A plate-tectonic speed limit? Nature 363, 216–217.
Meert, J.G., Van Der Voo, R., 1996. Paleomagnetic and 40Ar/39Ar study of the Sinyai dolerite, Kenya: implications for Gondwana Assembly. J. Geol. 104, 131–142.

Meert, J.G., 1999. A paleomagnetic analysis of Cambrian true polar wander. Earth Planet. Sci. Lett. 168, 131–144.
Meert, J.G., Nédélec, A., Hall, C., Wingate, M.T.D., Rakotondrazafy, M., 2001. Paleomagnetism, geochronology and tectonic implications of the Cambrian-age Carion granite, Central Madagascar. Tectonophysics 340, 1–21.
Meert, J.G., Powell, C.M., 2001. Assembly and break-up of Rodinia: introduction to the special volume. Precambr. Res. 110, 1–8.
Meert, J.G., 2003. A synopsis of events related to the assembly of eastern Gondwana. Tectonophysics 362, 1–40.
Meert, J.G., Nédélec, A., Hall, C., 2003. The stratoid granites of central Madagascar: paleomagnetism and further age constraints on neoproterozoic deformation. Precambr. Res. 120, 101–129.
Meert, J.G., Lieberman, B.S., 2008. The Neoproterozoic assembly of Gondwana and its relationship to the Ediacaran-Cambrian radiation. Gondwana Res. 14, 5–21.
Meert, J.G., Levashova, N.M., Bazhenov, M.L., Landing, E., 2016. Rapid changes of magnetic Field polarity in the late Ediacaran: linking the Cambrian evolutionary radiation and increased UV-B radiation. Gondwana Res. 34, 149–157.
Meert, J.G., Pivarunas, A.F., Evans, D.A.D., Pisarevsky, S.A., Pesonen, L.J., Li, Z.-X., Elming, S.-Å., Miller, S.R., Zhang, S., Salminen, J.M., 2020. The magnificent seven: A proposal for modest revision of the Van der Voo (1990) quality index. Tectonophysics 790, 228549.
Merdith, A.S., Collins, A.S., Williams, S.E., Pisarevsky, S., Foden, J.F., Archibald, D., Blades, M.L., Alessio, B.L., Armistead, S., Plavsa, D., Clark, C., Müller, R.D., 2017. A full-plate global reconstruction of the Neoproterozoic. Gondwana Res. 50, 84–134.
Mitchell, R.N., Evans, D.A.D., Kilian, T.M., 2010. Rapid Early Cambrian rotation of Gondwana. Geology 38, 755–758.
Mitchell, R.N., Kilian, T.M., Raub, T.D., Evans, D.A.D., Bleeker, W., Maloof, A.C., 2011. Sutton hotspot: Resolving Ediacaran-Cambrian Tectonics and true polar wander for Laurentia. Am. J. Sci. 311, 651–663.
Mitchell, R.N., Raub, T.D., Sillva, S.M., Kirschvink, J.L., 2015. Was the Cambrian explosion both an effect and an artifact of true polar wandeR? Am. J. Sci. 315, 945–957.
Moloto-A-Kenguemba, G.R., Trindade, R.I.F., Monié, P., Nédélec, A., Siqueira, R., 2008. A late Neoproterozoic paleomagnetic pole for the Congo craton: Tectonic setting, paleomagnetism and geochronology of the Nola dike swarm (Central African Republic). Precambr. Res. 164, 214–226.
Morel, P., 1981. Palaeomagnetism of a Pan-African diorite: a Late Precambrian pole for western Africa. Geophys. J. Int. 65, 493–503.
Mound, J.E., Mitrovica, J.X., 1998. True Polar Wander as a Mechanism for Second-Order Sea-Level Variations. Science 279, 534–537.
Mound, J.E., Mitrovica, J.X., Evans, D.A.D., Kirschvink, J.L., 1999. A sea-level test for inertial interchange true polar wander events. Geophys. J. Int. 136, F5–F10.
Nairn, A.E.M., Perry, T.A., Ressetar, R., Rogers, S., 1987. A paleomagnetic study of the Dokhan volcanic formation and younger granites, eastern desert of Egypt. J. Afr. Earth Sc. 1983 (6), 353–365.
Pisarevsky, S.A., Murphy, J.B., Cawood, P.A., Collins, A.S., 2008. Late Neoproterozoic and Early Cambrian palaeogeography: models and problems. Geol. Soc., London, Spec. Publ. 294, 9–31.
Rapalini, A.E., 2006. New late Proterozoic paleomagnetic pole for the Rio de la Plata craton: Implications for Gondwana. Precambr. Res. 147, 223–233.
Rapalini, A.E., Trindade, R.I., Poiré, D.G., 2013. The La Tinta pole revisited: Paleomagnetism of the Neoproterozoic Sierras Bayas Group (Argentina) and its implications for Gondwana and Rodinia. Precambr. Res. 224, 51–70.
Rapalini, A.E., Tohver, E., Bettucci, L.S., Lossada, A.C., Barcelona, H., Pérez, C., 2015. The late Neoproterozoic Sierra de las Ánimas Magmatic Complex and Playa Hermosa Formation, southern Uruguay, revisited: Paleogeographic implications of new paleomagnetic and precise geochronologic data. Precambr. Res. 259, 143–155.
Rapalini, A.E., 2018. The Assembly of Western Gondwana: Reconstruction Based on Paleomagnetic Data. Geology of Southwest Gondwana. Springer 3–18.
Raub, T., Kirschvink, J., Evans, D., 2007. True polar wander: Linking deep and shallow geodynamics to hydro-and bio-spheric hypotheses. Treatise on Geophysics 5, 565–589.
Reeves, C.V., de Wit, M.J., Sahu, B.K., 2004. Tight reassembly of Gondwana exposes Phanerozoic shears in Africa as global tectonic players. Gondwana Res. 7, 7–19.
Robert, B., Besse, J., Blein, O., Greff, M., Baudin, T., Lopes, F., Meslouh, S., Belbadaoui, M., 2017. Constraints on the Ediacaran Inertial Interchange True Polar Wander Hypothesis: a New Paleomagnetic Study in Morocco (West African Craton). Precambr. Res. 295, 90–116.
Robert, B., Greff-Lefftz, M., Besse, J., 2018. True Polar Wander: A Key Indicator for Plate Configuration and Mantle Convection During the Late Neoproterozoic. Geochem. Geophys. Geosyst. 19, 3478–3495.
Robert, B., Domeier, M., Jakob, J., 2020. Iapetan Oceans: An analog of Tethys? Geology 48, 929–933.
Rose, I., Buffett, B., 2017. Scaling rates of true polar wander in convecting planets and moons. Phys. Earth Planet. Inter. 273, 1–10.
Sahoo, S.K., Planavsky, N.J., Jiang, G., Kendall, B., Owens, J.D., Wang, X., Shi, X., Anbar, A.D., Lyons, T.W., 2016. Oceanic oxygenation events in the anoxic Ediacaran ocean. Geobiology 14, 457–468.
Santos, E., Santos, L., 2019. Reappraisal of the Sumé Complex: geochemistry and geochronology of metaigneous rocks and implications for Paleoproteorozoic subduction-accretion events in the Borborema Province, NE Brazil.
Santos, L.D.L., Dantas, E., Cawood, P., Lages, G.D.A., Lima, H., dos Santos, E., 2018. Accretion Tectonics in Western Gondwana Deduced From Sm-Nd Isotope Mapping of Terranes in the Borborema Province, NE Brazil. Tectonics 37, 2727–2743.
Schmidt, P.W., Clark, D.A., Rajagopalan, S., 1993. An historical perspective of the early palaeozoic APWP of Gondwana: New results from the early Ordovician Black Hill Norite, South Australia. Explor. Geophys. 24, 257–262.
Schmidt, P.W., Williams, G.E., 1996. Palaeomagnetism of the ejecta-bearing Bunyeroo Formation, late Neoproterozoic, Adelaide fold belt, and the age of the Acraman impact. Earth Planet. Sci. Lett. 144, 347–357.
Schmidt, P.W., Williams, G.E., McWilliams, M.O., 2009. Palaeomagnetism and magnetic anisotropy of late Neoproterozoic strata, South Australia: implications for the palaeolatitude of late Cryogenian glaciation, cap carbonate and the Ediacaran System. Precambr. Res. 174, 35–52.
Schmidt, P.W., Williams, G.E., 2010. Ediacaran palaeomagnetism and apparent polar wander path for Australia: no large true polar wander. Geophys. J. Int. 182, 711–726.
Schmidt, P.W., 2014. A review of Precambrian palaeomagnetism of Australia: Palaeogeography, supercontinents, glaciations and true polar wander. Gondwana Res. 25, 1164–1185.
Schmitt, R.D.S., Fragoso, R.D.A., Collins, A.S., 2018. Suturing Gondwana in the Cambrian: The Orogenic Events of the Final Amalgamation. In: Siegesmund, S., Basei, M.A.S., Oyhantçabal, P., Oriolo, S. (Eds.), Geology of Southwest Gondwana. Springer International Publishing, Cham, pp. 411–432.
Silva, P., Henry, B., Marques, F., Madureira, P., Miranda,, 2006. Paleomagnetic study of the Great Foum Zguid Dyke (southern Morocco): a positive contact test related to metasomatic processes. Geophys. Res. Lett. 33.
Sohl, L.E., Christie-Blick, N., Kent, D.V., 1999. Paleomagnetic polarity reversals in Marinoan (ca. 600 Ma) glacial deposits of Australia: implications for the duration of low-latitude glaciation in Neoproterozoic time. Geol. Soc. Am. Bull. 111, 1120–1139.
Stern, R.J., 2005. Evidence from ophiolites, blueschists, and ultrahigh-pressure metamorphic terranes that the modern episode of subduction tectonics began in Neoproterozoic time. Geology 33, 557–560.
Stern, R.J., 2008. Neoproterozoic crustal growth: the solid Earth system during a critical episode of Earth history. Gondwana Res. 14, 33–50.
Tohver, E., D'Agrella-Filho, M.S., Trindade, R.I.F., 2006. Paleomagnetic record of Africa and South America for the 1200–500 Ma interval, and evaluation of Rodinia and Gondwana assemblies. Precambr. Res. 147, 193–222.
Tohver, E., Trindade, R.I.F., Solum, J.G., Hall, C.M., Riccomini, C., Nogueira, A.C., 2010. Closing the Clymene ocean and bending a Brasiliano belt: evidence for the Cambrian formation of Gondwana, southeast Amazon craton. Geology 38, 267–270.
Tohver, E., Cawood, P.A., Rosselo, E.A., Jourdan, F., 2012. Closure of the Clymene Ocean and formation of West Gondwana in the Cambrian: evidence from the Sierras Australes of the southernmost Rio de la Plata craton, Argentina. Gondwana Res. 21, 394–405.
Tohver, E., Trindade, R.I., 2014. Comment on "Was there an Ediacaran Clymene Ocean in central South America?" by UG Cordani and others. Am. J. Sci. 314, 805–813.
Torsvik, T.H., Meert, J.G., Smethurst, M.A., 1998. Polar wander and the Cambrian. Science 279, 9.
Trindade, R.I.F., Font, E., D'Agrella-Filho, M.S., Nogueira, A.C.R., Riccomini, C., 2003. Low-latitude and multiple geomagnetic reversals in the Neoproterozoic Puga cap carbonate, Amazon craton. Terra Nova 15, 441–446.
Trindade, R.I.F., D'Agrella-Filho, M.S., Babinski, M., Font, E., Brito Neves, B.B., 2004. Paleomagnetism and geochronology of the Bebedouro cap carbonate: evidence for continental-scale Cambrian remagnetization in the São Francisco craton, Brazil. Precambr. Res. 128, 83–103.
Trindade, R.I.F., D'Agrella-Filho, M.S., Epof, I., Brito Neves, B.B., 2006. Paleomagnetism of Early Cambrian Itabaiana mafic dikes (NE Brazil) and the final assembly of Gondwana. Earth Planet. Sci. Lett. 244, 361–377.
Trindade, R.I.F., Amaral, C.D., 2017. Revisiting the Puga pole (Amazon Craton). 8th Nordic Paleomagnetism Workshop., Leirubakki, Iceland. Abtract Volume.
Van der Voo, R., 1990. The reliability of paleomagnetic data. Tectonophysics 184, 1–9.
Van Schmus, W., Oliveira, E., Da Silva Filho, A., Toteu, S., Penaye, J., Guimarães, I., 2008. Proterozoic links between the Borborema province, NE Brazil, and the central African fold belt. Geol. Soc., London, Spec. Publ. 294, 69–99.
Van Schmus, W.R., Kozuch, M., de Brito Neves, B.B., 2011. Precambrian history of the Zona Transversal of the Borborema Province, NE Brazil: Insights from Sm–Nd and U-Pb geochronology. J. S. Am. Earth Sci. 31, 227–252.
Vandamme, D., 1994. A new method to determine paleosecular variation. Phys. Earth Planet. Inter. 85, 131–142.
Vauchez, A., Neves, S., Caby, R., Corsini, M., Egydio-Silva, M., Arthaud, M., Amaro, V., 1995. The Borborema shear zone system, NE Brazil. J. S. Am. Earth Sci. 8, 247–266.
Williams, G.E., 2008. Proterozoic (pre-Ediacaran) glaciation and the high obliquity, low-latitude ice, strong seasonality (HOLIST) hypothesis: principles and tests. Earth Sci. Rev. 87, 61–93.
Wood, R., Liu, A.G., Bowyer, F., Wilby, P.R., Dunn, F.S., Kenchington, C.G., Cuthill, J.F. H., Mitchell, E.G., Penny, A., 2019. Integrated records of environmental change and evolution challenge the Cambrian Explosion. Nat. Ecol. Evol. 3, 528–538.
Youbi, N., Ernst, R.E., Söderlund, U., Boumehdi, M.A., Lahna, A.A., Tassinari, C.C.G., El Moume, W., Bensalah, M.K., 2020. The Central Iapetus magmatic province: An updated review and link with the ca. 580 Ma Gaskiers glaciation, Mass Extinctions, Volcanism, and Impacts: New Developments. Geological Society of America Special Papers.
Zijderveld, J., 1967. AC demagnetization of rocks: analysis of results. Methods i Paleomagnetism 3, 254.
Zijderveld, J.D.A., 1968. Natural remanent magnetizations of some intrusive rocks from the Sør Rondane Mountains, Queen Maud Land, Antarctica. J. Geophys. Res. 1896–1977 (73), 3773–3785.